JIMMA UNIVERSITY

JIMMA INSTITUTE OF TECHNOLOGY

SCHOOL OF GRADUATE STUDIES

SCHOOL OF MECHANICAL ENGINEERING

ANALYTICAL AND NUMERICAL ANALYSIS OF FATIGUE LIFE ESTIMATION OF
SPLINED SHAFT BY USING FINITE ELEMENT METHOD

Jimma Institute of Technology, School of Mechanical Engineering in partial
fulfillment of the requirements for the degree of master of science program in design
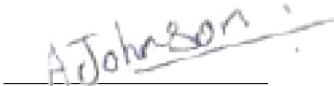of mechanical system

By
Ashagre Abebe

November 22, 2022
Jimma, Oromia, Ethiopia

Declaration

I, Ashagre Abebe Godana declare that this thesis entitled as, **"Analytical and numerical analysis of fatigue life estimation of the splined shaft by using Finite Element Method"** is my original work and that it has not been presented and will not be presented by me to any other university for similar or any other degree award. I also declare that all information in this document has been obtained and presented under academic rules and ethical conduct; as required by these rules and conduct, I have fully cited and referenced all materials and results that are not original to this work.

Name	**Signature**	**Date**
Ashagre Abebe		*22/03/2015*
(Student)		

As master's research advisors, we certify that we have read and evaluate this MSc thesis entitled as **"Analytical and numerical analysis of fatigue life estimation of the splined shaft by using Finite Element Method"** is submitted by Ashagre Abebe Godana our supervisorship as university main and co-advisors respectively.

Name	**Signature**	**Date**
Dr. Johnson	*A Johnson*	*21/03/2015*
(Main Advisor)		
Addisu Elmariam		*21/03/2015*
(Co-Advisor)		

Approval sheet

We, the undersigned members of the board of examiners of the final report by Ashagre Abebe Godana have read and evaluated this thesis entitled, **"Analytical and numerical analysis of fatigue life estimation of the splined shaft by using Finite Element Method"** and examined the candidate. This is therefore to certify that the thesis has been accepted in Partial Fulfillment of the Requirements for the Degree of Masters of Science in Mechanical Engineering (System Design of Mechanical Engineering)

Name	**Signature**	**Date**
Ashagre Abebe (Student)		22/03/2015
Dr.Johnson (Main Advisor)		21/03/2015
Addisu Klmariam (Co-Advisor)		21/03/2015
Abiyou Solomon (Internal Examiner)		22/03/2015
Dr Hailu Shimels (External Examiner)		12/05/2022
Firew Tullu (ChairPerson)		29/03/2015

ABSTRACT

The splined shaft is a significant component in the power plant and automobile industries because it performs two functions: it acts as an anti-rotational device or transmits torque to another device. This study deals with the splined shaft of the Howo 336 HP dump truck, which exists at the end of the driveshaft to transmit the torque with its version of the splines (i.e., splined hub) through a connection between involute spline contact faces. When continuous torque operation occurs, the stress becomes maximum at those contact surfaces, which leads to micro-pitting failures and reduces the fatigue life of the component. Therefore, various parameters leading to the initiation of such pits have been determined because once the flank surface fails, it cannot be restored and easily made for re-manufacturing to be reused again. To analyze them, both splines' CAD models (shaft and hub) were designed by Solid Work 2020 Premium based on the ANSI B92.1 involute spline manual, and the numerical simulation was done by ANSYS Workbench 19.2. Thus, the Hertz contact stress equation was used to calculate the influence of contact stresses under various flank surface loading conditions for the surface affecting factors called coefficient of friction, surface fatigue strength factor, and surface finishing process with its roughness. As a result, with a minimum variation of 5.9 %, the contact stress in an involute splined shaft agrees with the analytical contact stress calculated by Hertz stress. So, surface contact stress increases with higher friction in the area of contact and better surfaces that have less roughness, resulting in high fatigue strength. The results showed that when the surface load increases the surface fatigue life will decrease for given initial surface roughness. Meanwhile, on the analysis of the surface manufacture process due to the allowable fatigue life cycle for the various loading conditions, the mirror polished surface finishing process has high cycle fatigue among them. Then, within this surface finishing process, the flank surface of the fatigue life of the component can be improved.

Keywords: Coefficient of friction, Contact stress, Fatigue strength factor, Surface finishing factor, and Surface roughness

ACKNOWLEDGEMENT

First, I would like to give my endless thanks to the almighty God for his Mercy and help as his wish from the beginning. Next to this, I would like to give great thanks also to my main Advisor **Johnson Santosh (Assistant Professor)**, and second advisor **Addisu K/Mariyam (MSc.)** to help me by guiding the direction of this work.

And I would like to acknowledge and appreciate all my friends and teachers who have played a valuable role in my work by sharing supportive materials, data, information, and concrete ideas when I get confused and lost.

Finally, and most importantly, I want to convey my heartfelt gratitude to my family for their unwavering encouragement, patience, and unwavering support during my studies. And also especial thanks to my wife **Meaza Mekuriya** for all of her kind advice and dedication to my education next to my mom **Birtukan Gebure**. If it weren't for you, I wouldn't be who I am today or where I am today. I express my heartfelt gratitude to everyone who helped me during this research for their unfailingly kind support and assistance.

Table of Contents

List of Figures

List of Tables

ACRONYMS AND ABBREVIATION

K_t	Tangential friction
K_f	Fatigue strength factor
σ_c	contact stress
σ_y	Yield stress
a	Contact area
SN	Stress-cycle diagram
ANSI	American National Standard Institute
C_v	Effective clearance of splined mesh
FEM	Finite Element Method
TCA	Tooth Contact Analysis
CV	Constant velocity joints
AGMA	American Gear Manufacture Association
R_e	External spline radius
R_i	Internal spline radius
N	Number of cycles
p(x)	Contact pressure as a function of x-position
CAE	Computer Aided Engineering
v_1, v_2	Poisson's ratios
E_1, E_2	Young's modulus of Elasticity
a	Half width of the ellipse
CONTA	Contact and Targetted surfaces
R_a	Average surface roughness
N	Number of splines
SLC	Surface Loading Condition

1. INTRODUCTION

This chapter comprises eight sections. Thus, section 1.1 to 1.5 contains and describe a brief background of the splined shaft with relative descriptions such as; the main causes that motivated to study, the statement of the problem, the clearly stated research questions, and the objectives of the study. Section 1.6 and 1.7 contains the significance and scope of the study respectively. Lastly, Section 1.8 mentions a flow of brief thesis outlines (organization of the study).

1.1 Background of the study

In the world, there are different modes of transportation. Those are air, water, and land transport, which includes rails or railways, roads, and off-road transport. Such transportation uses some known components to produce power efficiently for the desired parts. Among these modes, road transport is the most cost-effective and convenient mode of transportation. It shares many mechanical components to transmit torque, such as gearboxes, driveshafts, springs, clutches, wheels, and so on [11]. Among those components, a driveshaft is one of the great functional components that play an important role in transmitting engine power to the rear wheels and pushing the vehicle forward and backward by employing various internal and external spline connections . Meanwhile, all on-road cars nowadays use rigid power axles to deliver power from the transmission (engine) to the wheels. Of the various power transmitter elements in cars, the splined shaft slot is the major one with the same hub connection from the gearbox [30].
A variety of aspects and joints are connected to transmit the torque that comes from the engine power of the vehicle. To perform this mechanism, special elements are needed, so-called splined meshes. It transmits by means of various joints which exist on it, such as universal joints (U-joint), constant velocity joints (CV), bearings, smooth and rough-sided inner and outer circular-shaped shafts, and so on [34]. All the splined meshes are commonly used in power transmission systems by connecting rotating and non-rotating parts, such as a shaft, and acting as a linear guide or otherwise transmitting torque and providing anti-rotation [3].
Instead of a key, these splined meshes are used as a series of projections, and their slots are used to keep cylindrical fitted machined-provided slots from rotating relative to one another, and a splined hub, gear, bearing, or other mating component is required to fit with splined slots. So, splined shafts are several integrated keys, which

are made with different manufacturing mechanisms and are fitted with another mating bore, called a splined hub slot. These slots are constructed as a series of keys that are milled into the shaft and broached onto the hub [31].

The designation of a splined profile is the base circle diameter, pitch circle diameter, and number of teeth, and they are known as the primary terms for the profile generation. Thus, the stress attitude and pitch circle are important considerations for spline cutting, especially in industries where splined meshes are more common [5].

This splined shaft is very susceptible to torsional shock and fatigue loads, which considerably affect the component's life. It's familiar as the grooved areas at the end of the driveshaft, as shown in Figure 1.1 , which exist at the top of the driveshaft to help connect non-rotating parts with rotating ones, which is called a splined hub or coupling.
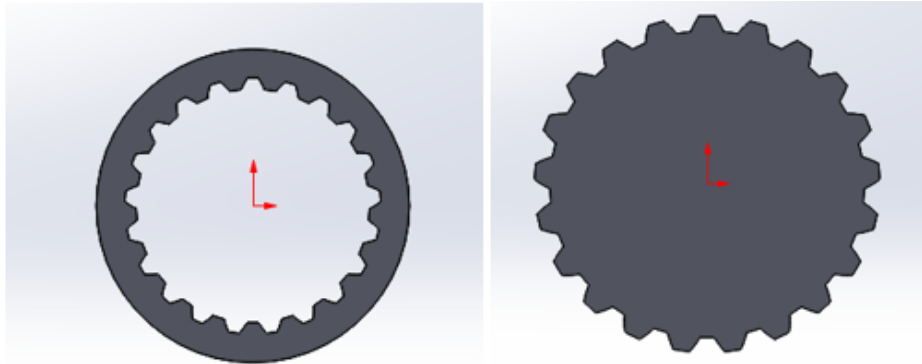
Figure 1.1: Internal and external splined shaft and hub projections

In comparison to another key-way drive, these splined meshes that shared the load have a longer fatigue life. Generally, these shafts are most commonly used in three types of applications.

- For coupling shafts when relatively heavy torques are to be transmitted without slippage,

- For transmitting power to slidably mounted or permanently fixed splines, pulleys, and other rotating members, and

- For meshing with such related hub parts, changes in the backward and forward movement position.

The splines are integrated keys on the end of an automobile driveshaft that mesh with grooves in a matched mating piece used to transfer the power. It is also that the splined shaft is considered a rotating machine element with a circular cross-section that is used in mechanical equipment and machines to transmit rotary motion and power. The other elements are called bearings, flywheels, gears, clutches, and other machine elements that are typically mounted on the shaft and aid in power transmission.

In this study, the slot parts of the splined shaft connection are considered, which exist at the end face of the driveshaft in the Howo 336 HP dump truck torque transmitter as shown in Figure 1.2. But this study was done by connecting only the input part of the splined connections with the splined hub together. In the meantime, the connection of both splined slots is taken into account.

Figure 1.2: The splined shaft of How Dump truck [From the garage maintenance]

1.1.1 American National Standards Institute (ANSI) for Involute Splines shafts

The American National Standard Institute (ANSI) give the desired information based on different rotational applications. These type of splines or multiple integrated keys are similar in form to internal and external involute splines. Such splines can be precisely spaced, have their greatest strength at the base, and are self-centering, balancing the bearing and stresses. The generic practice is to structure the exterior splines both via hobbing, rolling, or on a tool's shaper [9].

The standard acknowledges that effective criteria for the spline from the tip of the slots to the form diameter must be met for appropriate assembly between matching splines. Many ANSI features are retained, but the common manual for such shape components is ANSI B92.1 (see Figure 5.1), and it's been selected for this study.

1.1.2 The hub or coupling mesh to the splined shaft

A splined hub is a machine component that transmits torque between two components that are not permanently connected. It is also considered as a fixed element before producing the power to the desired wheels, which also allows them to be employed in a wide range of applications, from driveshafts to clutches, in the automobile sector.

With same manner, some of the literature deals failures of splined hub that investigates experimentally and theoretically due to splined shaft connections considered as the spline tooth profile [4, 8]. It is also useful for attaching and disconnecting elements in a rotating assembly because of its ability to move translationally while rotating. As shown in Figure 1.3 , the design includes a slot cut out of both the axle and the hub with a key inserted to limit rotational movement between the two components.

When operating power, the high concentration of stress acts on the flank face of the hub because it has a contact edge with splined shaft. Meanwhile, in this study, the outer part of the failure may not be considered, rather only the internal contact parts of splined shaft.

1.1.3 Types of the splined shaft

There are different types of splined shafts to transfer smooth torques with different tooth arrangements. Each type of its projection is differing on applications to desired functions. Those are:

I. Parallel splined shaft: A parallel splined shaft would feature square-shaped ridges or teeth. These splines have straight-sided slots with equal spacing. As seen in Figure 1.3 below, the key-way on the shaft have the same slot thickness at every location measured radially away from the axis of rotation. Except for the fact that the keys are built into the shaft and evenly placed all around, this kind of spline is identical to a key-way drive.

The major and minor diameter of the internal splines, or the outside diameter of the shaft and the minor diameter of the shaft, can serve as the piloting feature. On this type of splined shaft the fits are permanent and the geometries are not involute profile, to slide when not under load [17].

Conversely, parallel key splines feature grooves that are evenly spaced and all parallel in both the axial and radial orientations. They can be cold-rolled or cut. On this shaft, the flank face is directly contacts with flank surface of parallel hub throughout faces and it has an equal width and height.
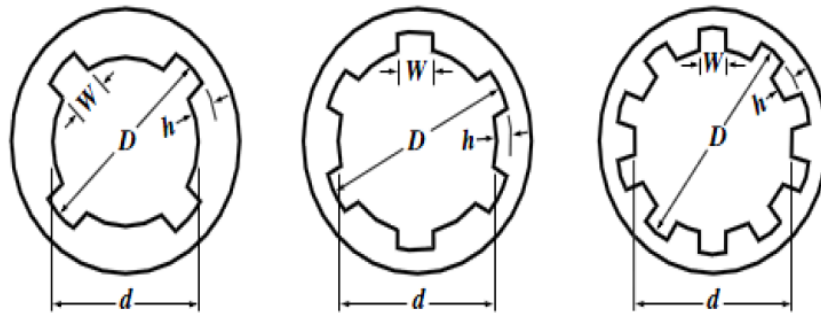
Figure 1.3: Parallel Splines key with 4, 6, and 8 slots [6]

II. Involute splined shaft: An involute splined shaft (so-called evolvent) is a curve created from another provided curve by attaching an imaginary taut string to the supplied curve and tracing its free end as it is wound onto that given curve. A spline slots with an involute profile is known as an involute spline [12] and [29].

Due to their strength and ease of cutting and fitting compared to straight-sided splines, involute splines are the most used type. Hobing or a spline shaper can be used to create external splines and broaching or a spline shaper can create inside splines. It has tapered ridges along the shaft, which help in lowering the stress concentrations during gear operation [16].

Such splines are commonly used in the automotive and other product manufacturing industries with profiles similar to those of other involute and non-involute gear teeth based on ANSI B92.1 standard specifications [9].

During this operation, the element leads to failures after working a long time, and various failure patterns act on it. It has greater torque-transmitting capacity than any other type of splined gear, especially in the automobile industry. It can be produced by the same technique and equipment as used to cut gears, and they have a self-centering action under load even when there is backlash between mating members [6].

The teeth have an involute form, just like another involute gear tooth, as shown in Figure 1.4 below. The involute splined gear forms feature three pressure angles of 30 degrees, 37.5 degrees, and 45 degrees, as indicated in Appendix A and the ANSI B92.1 standard manual.

Hong, J. Talbot et.al, [10] suggested expanding the formulations of elastic bodies in contact and developing a semi-analytical load distribution model for side-fit involute splines. As a result, any manufacturers and designers must be considered the surface loading conditions before providing for the desired applications of it. The Figure 1.4 shows that internal external splined shafts and splined hubs with equal number of key-ways those uploaded from the garage and SolidWork for only contact surfaces.
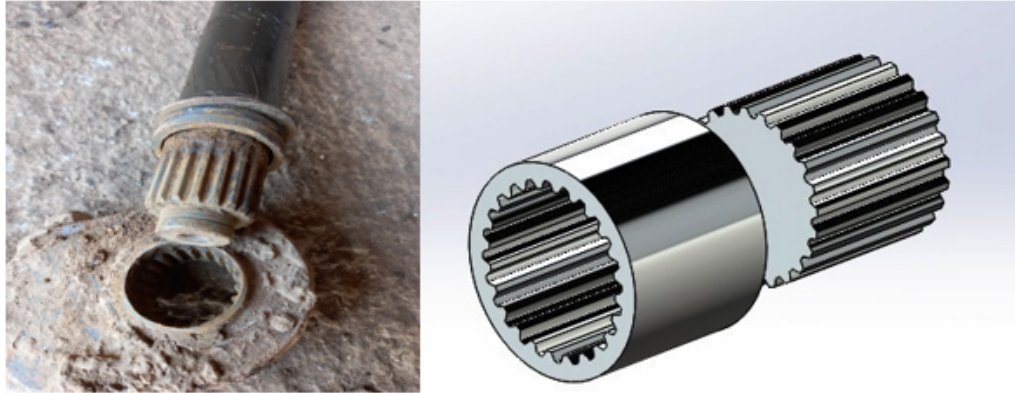
Figure 1.4: Exploded drawing of internal and external involute splined shaft

In mechanical power driving systems, a common method for transmitting rotational motion and torsion from one rotating (moving) component to another (i.e., a fixed spline key) is the splined shaft described and discussed in this study.

An external splined shaft and internal splined hub are to be assembled or manufactured with the same number of slots which is securely fitted together along the same rotational axis to form a splines joint. This shape is determined by parametric equation and Archimedes's principles for the involute shape geometry. The involute of a circle forms a shape that resembles an Archimedes spiral, which is mentioned on chapter three to develop the profile as shown Figure 1.5.
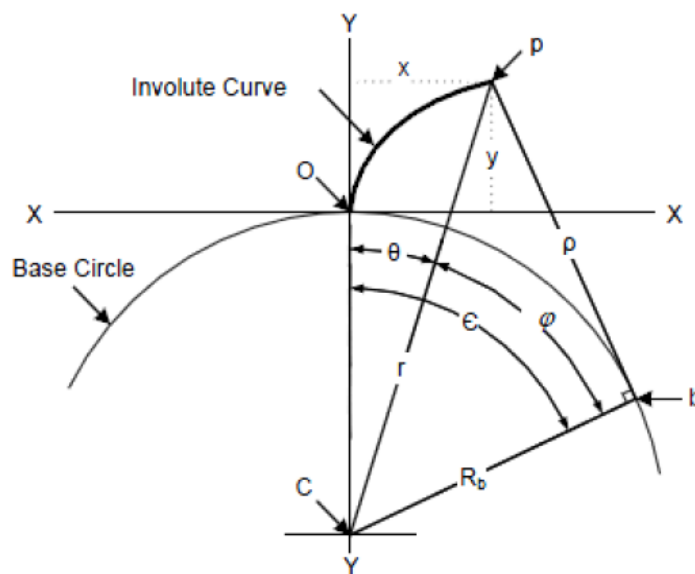
Figure 1.5: Generation of Involute Spline curve [11]

Such Involute Splined shafts have broader pressure angles and shorter key heights, although they frequently have greater strength. Nevertheless, this spline meshes frequently fails as another splined shaft due to fretting wear, corrosion fatigue, and tooth breakage in due to varying surface loading conditions.

II. Crowned splined shaft: This type of shape component is same as involute splined shaft, but it has a short crowned key and crowned shape. with tooth classification, the geometries are not involute shape. To correct for angular misalignment, crowned splines are often involute splines with topped or curved keys. These specific splined shafts have keys that taper or smooth out as they approach the splines terminal face. This permits angular misalignment when the keys are operating. Figure 1.6 illustrates the non-involute slots form of the spline and surfaces effects due to variable loading conditions [3] .

The key may be formed at end of the component or center of the component which is depends on plant installing foe the specific purpose. Based on arrangements (for fitting purpose) the internal crown keys has spaces with the same included angle as the external detail's keys, which are shaped like an included angle. While, this crowned splines can manage misalignment's of up to 5 degrees, straight-keyed splines can only handle tiny misalignment's of less than 1 degree, and their failure patterns resemble zig-zag patterns due to the angle formed [8].
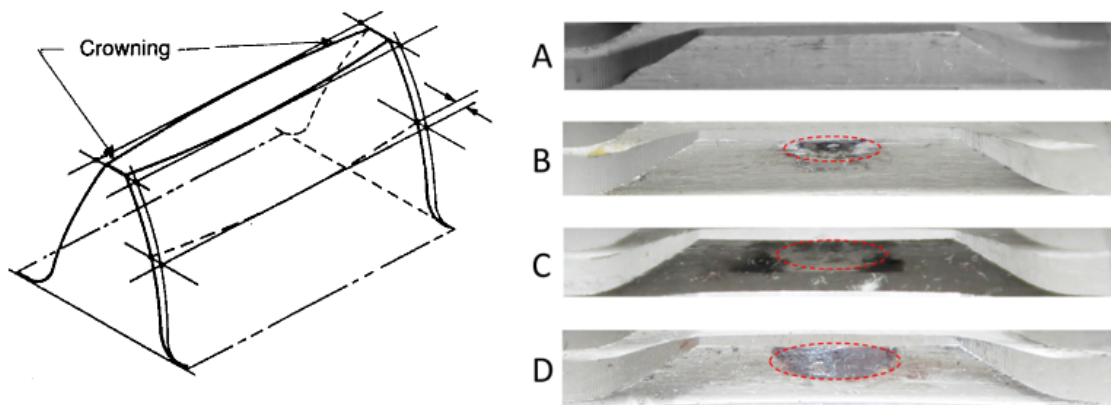
Figure 1.6: Crown splined shaft and flank surface failures [3]

III. Serration splined shaft: Serration splined shafts are called non-involute splined shafts. Such key-ways will be installed on the hub itself since the splined key-ways will be provided for on desired application with an angle. Thus, Serrations feature

angled flanks rather than straight ones, as seen in the Figure 1.7 below. The serra-
tions' main benefit is that they produce self-centering splines since the angles they
form flank the shafts and the hub. Typically, flank angles range from 50° to 90°.
Serration splines are utilized in valve shafts, instrument drives, and similar compo-
nents. Meanwhile, its disadvantage is that they can only be utilized for low torque
applications due to their comparably small teeth. When an involute form would not
improve strength, serrations are typically utilized on drives with lower diameters.[8].
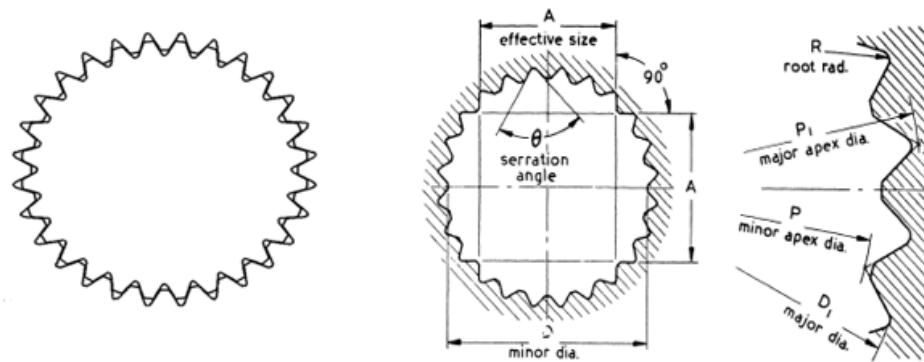
Figure 1.7: Serration Splined shaft [8]

V. Helical spline shaft: A shaft with helical splines would have either parallel or in-
volute splines where the ridges create a pattern of helixes across and around the shaft.
These zig-zag-style tooth splines have a specified lead and helix angle and can have
parallel or involute key-way shapes as seen in Figure 1.8.

Splines of this type are used as an application element in any large form or machinery
to transmit angular rotation. A straight spline may result in driving shaft breakage in
places other than the spline in drives where the spline shaft may become a torsional
wound-up. This is because complete contact along the driving side of the slots is pro-
duced by the load applied over the whole length of the spline. With the addition of
the spline, this load sharing spreads the rotating torque over a more extended portion
of the shaft.

These helix multiple tooth splines or multiple helix keys may assemble as internal
and external parts in terms of form for angular motions. with the same manner, both
the external and the internal splines are typically formed either by hobbing, rolling,
or using a gear shaper. The fit is controlled by varying the exterior spline while main-
taining the inside splines basic dimensions.
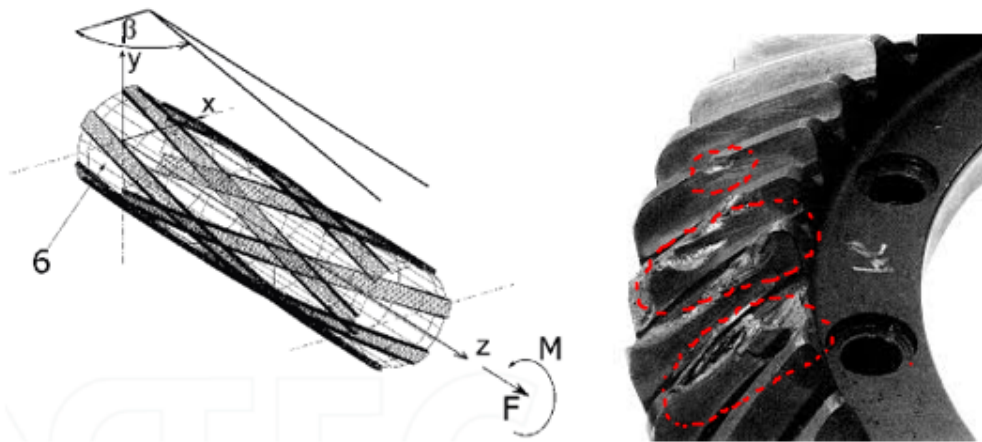
Figure 1.8: Helical splined shaft [14]

1.1.4 Functions of a splined shaft

To transfer the torques from the source to be delivered component the assembled component is needed, one of them is a key-ways, the integrated key-ways are so-called splined shafts, or with the help of a hub. A hub mounted on a shaft, for example, would have female splines that interlock with male splines on the shaft [12]. The transmission of motion between two shafts was accomplished through the use of mechanical connections, including splines.

According to the spline's teeth arrangement, there are two types of splines. Those are Internal splines and External splines. They are designed to allow the shaft to engage with the hub over the entire circumference. Unlike splines, the point of contact between mating splines remains constant and multiple splines engage to transmit torque; therefore, splines are ideal for applications involving high torque loads.

The basic splined shaft's operation is to mate with a female version of it, or interlock, to transfer rotary movement [3, 4]. When working with a bearing with an internal spline gear mechanism, it can also serve as a linear guide. The interaction and interlocking of the gears and shaft would be crucial. As an example, spline couplings are used in wheel rotating systems by transmitting the torques smoothly and braking systems for large industrial vehicles like the huge dump trucks used for mining operations. Exploded view of such torque transmitting application, which uses two sets of spline couplings or hub to provide high torsional power to the wheel.

Splines transfer smooth torque and speed from the shaft to the hub or vice versa. Furthermore, they prevent movement between them in a peripheral direction. Their

teeth can be straight-sided, with included angles, or involute. The transmission ratio between the shaft and the hub is 1:1 because their slots are directly met at one time, this means there is no variation between external and internal splines [4].

1.1.5 Application areas of the splined shaft

The transmission of motion between two shafts was accomplished through the use of one of the mechanical connections, called splines. In every industry, this kind of spline element is used so far to transmit desired torques, such as on heavy machines to transmit the torque smoothly, manufacturing companies, automobiles, aircraft, and so on [17, 31].

Typically, any splines are designed with shorter teeth and with large pressure angles than standard gears to carry higher loads. In general, the standard pressure angles for involute splines are 30, 37.5, and 45 degrees as mentioned in types of involute splined gear, while gears typically utilize pressure angles of 14.5, 20, and 25 degrees were for lower frictional applications such as spur gear components. So, involute splines are a special class of keys that do not engage in conjugate action or smooth continuous motion, but the key-ways in spline coupling remain fixed relative to each other [23].

One of the major application areas is on heavy-duty pieces of machinery, such as aircraft and off-highway trucks, special brakes are required to handle the high levels of torque. Because of the size of these machines, conventional disc brakes are inadequate; a brake containing several brake rotors is needed. These are commonly referred to as multi-disc brakes because it holds multiple friction plates and delivers the torque to each of them at once. An example of a multi disc brake can be seen in Figures 1.9.
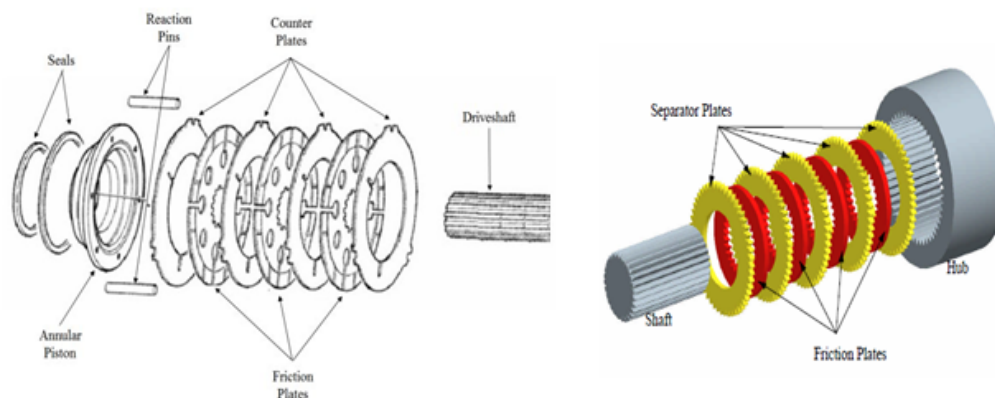
Figure 1.9: Exploded view of a simple multi-disk brake [10]

An axial force is applied to the outermost separator plates by a series of pistons placed

around the perimeter of the hub, causing the friction and separator plates to push together. This generates a braking motion, causing the hub and shaft to come to a halt relative to each other.

A normal multi-disc brake utilizes units of rotating friction and stationary separator plates and may additionally use coolant. A friction plate is positioned between every pair of separator plates. Thus, their function is similar to conventional disc brakes, in which the rotor is between a pair of brake pads. Both the friction and separator plates are usually made of steel and rotate with the help of splined key-ways as one.

Most gearboxes use two types of spline connections - permanent and temporary. Permanent splined key-ways are known as splined couplings of gearboxes, while temporary splined slots on gearboxes are called splined shafts [6].

1.1.6 Major Causes and failure modes of the splined shaft

The splined shaft is created using a variety of surface finishing processes, each of which has a unique surface roughness. These processes include broaching, shaping, milling, hobbing, rolling, broaching, and grinding. Those mechanisms are used to create internal and exterior splice slots. The suggested face of the splined shafts is normally subjected to various loads following the creation of the key-ways, such as cyclical loads, bending loads, and changing or vibratory loads (due to constant velocity installation). That is the main cause of the component's failure, especially on strain raisers where spline surfaces and roots. The majority of disasters occur inside the location where the splined slots are formed since this factor is operated or situated there to switch movement through it.

This tension very leads to the splined surface's failure. Most investigations addressed the most prevalent failure mechanisms seen in spline joints [2, 18]. Generally, the following failure modes mechanism can be drawn;

Surface wear fatigue: Also known as surface fatigue, wear is another factor of damage. It is the gradual removal or deformation of the material from the solid surfaces that [8]. Damage to the surface of the key-way can lead to a key-way/spline not being able to fully transmit to the torque level as designed. In addition, if the key-way/spline is damaged, the shaft and hub connection will not be fully transmitting to desired parts, See Figure 1.10.

Due to discontinuities, defects, the effects of surface finishing, and other major contributing stress raisers, the small pit crack nucleates propagate to the level of propagated pitting throughout. Before strain rises on the surfaces of it, various influence parameters must be considered to extend the life of it. This study details on such influence parameters.

Fretting corrosion fatigue: Fretting is both corrosion and a wear mechanism in which mating surfaces nominally at rest undergo small amplitude oscillatory motion, All such patterns fail to act by absorbing the water content of the lubricants, causing corrosion, particularly where two splines meet together [15]. This may happen when the nucleated cracks goes to propagate such small hole like shape or less crack will happened on the surface of splined meshes.

Tooth breakage: The majority of failures are caused by excessive spline slot surfaces loads, which result in root stresses that exceed the material's endurance limit. Under normal operating conditions, the shaft moves along the wheels due to external torques, though with some input profiles vibrations will occur on the splined faces, especially at the contacted surfaces. This leads to the most crushing failures. And also, when the external loads exceed the surface endurance limits, the key-way damage occurs at the slot contact surfaces, and then after it could be completely out of service by damaging the rest of the one [16], and [17].

Meanwhile, such failures (corrosion fatigue and tooth breakage)are not considered for this study because the component will not be reused again.

Figure 1.10: Failed shaft and hub with surface wear damage due to minor pitting

1.2 Motivation for research

A dump truck, often referred to as a dump trailer, dumper trailer, dump lorry, or simply a dumper, is used to transport coal as well as construction materials. This truck carries high loads with high torque transmission, when it has a high external load increased high torque with less speed is requested. In this study, spline mesh takes account of the surface contact to transmit smooth power, in this case, to estimate the fatigue life with cyclic loads.

Any machine component must be in good condition to perform the desired task effectively. One of the key parts used by the automotive industry to transmit torque is the splined shaft. This driveshaft's end-aligned component is also taken into consideration in this study because it is one of the key parts used in the automotive industry to transmit engine power directly to the rear wheels without any loss of efficiency. When the spline surface is in touch with the hub spline surface, which implies that power is transmitted via contact surfaces to the wheels and motion will occur.

As mentioned in the preceding section, when the faces of the spline slots are the most contact regions, crack initiation and propagation can occur, with the most common failure modes being surface wear, fretting corrosion fatigue, and tooth breakage. If the component fails on it, the component will be eliminated from there because there will not be a correct gap between the shaft and hub. Just after it fails, no long remanufacturing or re-surface finishing process takes place to replace it, because it does not fit with the hub dimensions. Even to replace it with a new one, high costs may be required.

1.3 Problem statement

In the engine torque transmission of the Howo 336 HP Dump Truck, the splined shaft plays a major role with its version to deliver the power to the rear wheels. This power is delivered by means of connecting both shaft and hub flank sections of the slots. In order to transmit such engine power, good surface conditions and high surface fatigue strength are needed for those slots to withstand surface fatigue failure due to occurring at high surface contact stress.

When the component is subjected to fatigue loading, the surface fatigue strength of an involute splined shaft and hub is more influenced by a variety of factors (such as ; surface contact stress raisers, surface fatigue strength factor, surface finishing process, and surface roughness). All these factors should be considered before starting the operation to resist the pitting formation easily and improve the fatigue life cycle of the slots, because these factors would happen just if the component is manufactured and going to operate.

If a spline surface fails, no remanufacturing or refinishing process will take place other than discarding and encouraging the replacement of the part and subsequent catastrophic failures. To overcome this problem, the parameteric study of surface factor is very important to improve the fatigue life cycle of the slots by investigating those factors due to different lateral surface contact stress, which play a significant role in improving the fatigue strength and surface finish performance by applying different

surface loading conditions.

1.4 Research questions

- How to make an involute flank profile for the splined key-ways parameters that are to be considered for the contact diagnosis?

- How do determine analytical and finite element methods to calculate the contact stresses for an involute splined mesh to the surface fatigue life analysis?

- What are the factors that influence the surface fatigue of an involute splined mesh, which results in surface fatigue?

- How does the involute spline mesh's fatigue life change under different stress circumstances depending on the key-way flank surface roughness?

1.5 Objectives of the study

1.5.1 General objective

- The general objective of this study is to investigate the contact stress and estimate surface fatigue life in rolling sliding contact of involute splined tooth effects by Finite Element Approach.

1.5.2 Specific objectives

- To model the external and internal involute splined key-ways by developing its parametric equation on Solid Works Premium 2020.

- To investigate the effect of involute splined meshes contact surface finish on fatigue life by Finite Element Method

- To study the overall effect of loading conditions on surface fatigue strength of the involute splined shaft.

- To verify the surface contact stress of analytical results with the Finite Element analysis.

1.6 Scope of the study

- The goal of this study is to conduct a parametric analysis to determine how the surface condition affects the life of the spline shaft/key-ways in the power transmission of the Howo 336 HP Dump Truck.

- No longer dynamic factors considered due to static surface loading.

- The study was limited to the impacts of the contact zone on the flank surface of the spline shaft that interfaces with the spline hub. The overall specifications/dimensions or other numerical informations were used from the standard manual of ANSI B92.1 for both connection parts.

- To control such a work environment, one of the best methods is experimental work, but it's so expensive works to fatigue tests. Thus, the current work is based on only Analytical and Numerical works, not including experimental setups rather than validation.

- Due to frictional and frictionless conditions, both splined shaft and hub are considered as contact and targeted surface respectively.

- There are various types of failures in the external and internal splined meshes which all are no longer addressed in this study than the contacting flank surface stress raisers of the component.

- For the purpose of validation, the simulation was done between the two pair components by taking the contact size as 0.15 and, for CONTA 170 and CONTA 174, the Tetrahedron meshing type is taken into account.

1.7 Significance of the study

- This study may help to assist mechanical designers to improve the parameters by depending on the provided results to reduce such losses that act on surfaces.

- The analysis was done on ordinary computers this is used to get what results in a short time and it can be used in areas where experimental setups are not available.

- The delivery of a great idea to do with the same approach to other such contact bodies, specifically other forms of machine gears in mechanical streams, helps any mechanical component that connects one with others at the surface.

- It helps to determine the remaining lifetime of the components at the surface of contacting bodies and plays a major role for coming researchers by giving mechanisms before starting the surface pitting formation.

1.8 Organization of the study

The thesis will be organized in to the following five chapters.

- Chapter One: Introduces the background of splined shaft (especially involute splined shaft), motivation for the study, Problem Statement, objectives of the study, Scope of the study, significance of the study and overall chapters organization are mentioned.

- Chapter Two: Consists of reviewed relevant research papers regarding splined shaft failures and its parameter influence on the fatigue life and the research gap from literature is explained.

- Chapter Three: In this chapter, there are four sections.

  - The first two sections detail the material specifications and definitions of the terminology, and the material mechanical specifications were considered briefly.

  - The second section is about the modelling and the parameters which are to be considered as input parameters to design and simulate it. Thus, all the terminologies formulae were considered in the SolidWork to model the spline.

  - The third section generally considers the analytic formulae for surface contact stress with pressure distribution along the contact spline length.

  - The last section, details overall numerical flows . which incorporates with analytical methods and boundary condition to send into the Ansys Workbench

- Chapter Four: The results which took into account the loading conditions discovered are addressed for the factor of fatigue strength, surface finishing, and so on are analyzed with loading conditions. Thus, all the results are addressed as stated in the problem statement respectively.

- Chapter Five: This chapter is dedicated to the conclusion, recommendation, and future works for the coming researchers based on mentioned overall results. Latly, the latest references and all basic informations are mentioned also in appendices.

2. LITERATURE REVIEW

The foundation for this thesis is provided by two sections. First, a summary of spline geometry and an explanation of Hertz contact theory are provided. After that, a review of previous studies is given in the fields of statistical modeling, finite element analysis, spline engagement, and deflections and stresses of key-ways. An overview of earlier studies is provided in this chapter. Even though some of the materials don't specifically mention splines, they are nevertheless relevant to this topic in some way. To create an analytical model that incorporates tooth geometry, changes, errors, deflections, stresses, and engagement, a thorough understanding of the topics covered is required. Meanwhile, the structure of review writing is based on methodological ideas rather than the chronological methods of literature surveys used in all of the reviews.

2.1 Historical perspective

One of the key pieces of a movable machine for transferring high torque power to desired elements is a splined shaft. It is one of the most crucial parts of a mechanical power transmission system, as well as in the majority of industrial rotating types of machinery, to convey power smoothly from the source of energy to the desired components. To date, numerous studies on splined key-ways modeling, parameters, and stress analysis have been conducted.

Additionally, all splined shaft and hub designs always take the involute shape of the key-ways into account while doing bending stress analysis, flat root stress analysis, calculation of dynamic loads, coupling load effects, vibratory analysis, and contact frictional analysis. All the results were handled in this chapter, but before the failure mode, the contact stress effects due to the surface finishing process were not considered here.

The overall considerations of this chapter comprise a summary of what previous research has been done to date. Although some of the sources do not address splines, in some ways they are pertinent to this study. An in-depth understanding of the subjects presented is necessary to develop an analytical model, which includes splined tooth geometry, parameter considerations, errors, tooth deflections, surface or flank and root stresses, and clear engagement. As each involute splined shaft in a transmission's power flow path enters and exits its key-way meshes, it is subjected to cyclic loading to transmit the desired torque, as stated in [15].

2.2 Spline geometry modifications

Splines frequently use design characteristics that are not specified in the ANSI B92.1 standards. Commonly, these features include large numbers of key-ways and low pressure angles. According to Xiangzhen Xue et al.[41], the variations for spline couplings with more than 100 key-ways should be computed using a 100-tooth coupling. Additionally, notes that splines with pressure angles of 14.5°, 20°, or 25° are more prone to wear because they are less stiff, leading to greater deflections.

The geometry is defined similarly to gear teeth in the case of the lower pressure angles. The height of the tooth is typically half that of gear teeth, which is the only difference. By making deeper cuts into the outer spline slots, more clearance is created. This allows for large amounts of coolant to be added to a cooling system. As of right now, most studies don't have the formulae or relationships that can predict how much the radius of curvature will change.

2.3 Splined shaft surface errors

The effective clearance is effected by four primary mistakes [11]. Lead variation need not be taken into account because of how thin the friction and separator plates are. The three remaining mistakes are variances in slot thickness, profile, and index. Tumpala Uma Santhosh [4] agreed that irregular key-ways profiles are a result of manufacture.

Backlash in mesh slots and effective clearance in spline key-ways are analogous. When O. Lyashuk [19] examined backlash in assembled key-ways, the study discovered that size variances and slots defects are the primary causes of backlash. The slots thickness allowance, which gives space for mounting, thermal development, and lubrication, is the cause of the size variances. Local differences in key-ways profile, spacing, and thickness are the main causes of surface key-ways mistakes.

The profile variation is any deviation from the required involute profile normal to the flank, according to the ANSI B92.1 standard [9]. A change in the profile can either result in a greater or lesser effective clearance. A higher change in profile leads to a lower clearance. An increase in clearance is the result of a negative fluctuation.

The key-ways clearance is also directly impacted by index differences. A single key-way's offset might be in either direction, increasing or decreasing clearance. Index errors are measured in relation to an unchanging reference, and their combined total is zero. surface-to-surface gap is a variant of index error. This is a mistake in the distance between adjacent key-ways.

2.4 Overall splined shaft failure and its parameters study

The splined key-ways have a great degree of durability and compactness. During the operations, various surface failures exist between two mating involute splined key-ways, and one of these component surface failures is due to cyclical loads, which are called fatigue failures, and almost all of the following citations are related to this concept. The finite element method is widely used for the analysis of splined shaft and correspondence for those failures (i.e., fatigue). There are the same behaviors on each key-ways because the ratio of the splined key-ways is 1:1, which means all the key-ways of the splined shafts are meeting at the same time without slipping [4]. The majority of this study has investigated the impacts of amending a single parameter or a subset of factors on surface contact analysis due to fatigue life. As a result, the following literature evaluations are generally divided into three categories: those are

- the effect of material on surface fatigue,

- the effect of surface conditions on surface fatigue, and

- the effect of operating loading conditions on surface fatigue.

One of the surface fatigues will happen due to fretting, which is also similar to brinelling [41]. The only difference is the patterns that exist on the flank of the surface. Both are caused by the surface loading condition, which forms sludge on splined shaft face at or near the contacting point.

Tae-Wan Ku [16], studied the surface effects of the tooth subjected to cyclic tooth axial strains as a result of its intermittent loading. It is focused on the involute internal splined shaft manufacturing by using the forward-backward extrusion forging process. Meanwhile, AISI 1035 carbon steel is used as a raw material. The internal spline at the upper head region has a three-dimensional one-sixteenth (1/16) symmetric feature, and in the same manner for the spur gear was one-thirty second (1/32) symmetric shape, due to the symmetric characteristics of the splined shaft. The determination of the minimum symmetric shape for assuming the boundary condition of the numerical simulation models and reducing the computation time of the two-stage cold forging was addressed. During the two-stage cold forging operations, the shear friction behavior was expected to be 0.098 between the tool components and the work-pieces.

Li-Hui Zhao, et.al. [14] proposed the variation of splined driveshaft failures at two different driveshaft places, especially in root stress concentration due to bending effects at the fillet region. This failure analysis also aids in predicting the effects that will

be evaluated during the involute splined shaft's remaining life period. Thus, fatigue-induced tooth breakage failures can occur under such loading conditions depending on the status of strains along the root region and the geometry of the root fillet. The chemical composition was analyzed for such materials as carbon steel, manganese, silicon, chromium, nickel, and molybdenum. The inquiry was divided into four phases to determine the root cause of the drive shaft fracture, such as fracture surface examination, material inspection, mechanical properties tests, and local contact stress analysis. The setup was done by bench-marks by cutting out the fractured parts of the splined shaft, while the stress distribution contours of the shaft and critical zones were based on the finite element analysis. However, from the collected data during the operation of 26000 Nm, this study only addresses a single applied loading condition, referred to as torque. The results show that critical zones exist at the right spline shaft's root, with a maximum stress magnitude of 954.3 MPa, which is consistent with the experimentally observed crack initiation zone.

Bodzas and Sandor [1] deliver the manufacturing techniques of internal and external splined shafts based on standard cutting machines and geometric illustration. And also, they developed the splined fitting to other design works. Milling and grinding technologies were used from the various manufacturing technologies and developed by mathematical models for both of them in this study. They define the technological parameters and the computed machine time for the manufacturing designing process and recommend their modeling technologies for the different shapes. As a result, the milling surface finishing is a major consideration concept in manufacturing operations to improve the lifetime of the components based on loading conditions.

Francesca cura, et.al [18], The study was proposed by considering the fretting wear due to surface loading conditions on the surface of crown splined couplings in real working conditions. Both surface fatigue and wear behavior were considered to achieve the component's optimization, as detailed. For the analysis of the crown splined coupling, 42CrMo4 alloy materials were used. And also, as concerns fatigue life, standard design methods consider only a part of the spline teeth to be in contact, and this leads to an underestimate of the component's life. They consider the wear kinematic conditions, called angular misalignment between the shafts and torques of delivered teeth deflection, caused by the relative sliding between engaging teeth. In this study, the fatigue damages are investigated experimentally and numerically. While the wear damages are investigated, they are only experimentally evaluated. The findings demonstrate that the actual component life is longer than that calculated using normal approaches when it comes to fatigue life. In terms of wear behavior, the findings reveal

that wear damage occurs whenever there is a relative motion between engaging teeth.

2.5 Spalling and pitting formation on flank surface of the splined shaft

Over the previous few decades, numerous splined shaft pitting investigations have been conducted. The surface fatigue life of the component is influenced by key material, gear geometries, heat treatment, case hardening, surface quality, surface roughness, lack of quality of lubrication, temperature, operating torque variation, operating speed variation, and so on.

When cyclic stresses in an involute splined keyways develop minor cracks at or below the surface of the tooth face, then pitting occurs. As the gear material fractures and is removed from the tooth, these small pits cracks will grow into larger holes, then failures start here. As the removed material causes more stress concentrations on the splined tooth face, the pit expands in size. Such a consideration was discussed in [17]. While, the criterion that determine keyways bending fatigue are confined to geometry, material, and loading levels, a wide number of variables interact to determine splined shaft contact fatigue conditions.

Kalathur Kumar, et.al,. [28], presented surface pitting on the splined gear tooth. Thus, studied as one of the types of surface fatigue in which metal surfaces develop pits or voids. Pits can start as small as a pinhead or even smaller. Pitting will proceed if left uncontrolled until surface metal fragments break free from a component and enter the axle lubricating system. The instantaneous normal stresses coupled with the corresponding surface shear stresses caused by instantaneous traction result in multiaxial stress states below the involute splined tooth surface, which causes pitting failures. The splined shaft pitting, which is acted on the surface of the spline, is still one of the prevalent failure modes faced by the shaft of transaction systems.

According to Rabish Kumar et al. [7], surface micro-pitting is usually connected to the extreme roughness of the ground and hardened steel gears, which causes surface stress concentration. By Considering high surface roughness, the lubricating film thickness is often smaller than the combined average roughness of the surfaces, particularly when the gear operates with high loads and then high vibrational speeds. The degree of lubrication ceases to be Electra hydro dynamic (EHD) under these conditions and becomes mixed film lubrication or even boundary film lubrication: a significant part of the contact load is borne by direct contact between the roughness features of the meshing teeth surfaces. The results show that the adequate consideration of mixed film lubrication is therefore of primordial importance when dealing

with micro-pitting.

O. Lyashuk et al. [19], Examines the surface spalling which is on the splined shaft surface failures and theoretically details about surface spalling and sub surface spalling, because it is the term for when wear fatigue causes a component's solid surface to crack into chips or fragments. In this study, wear fatigue spalling, a form of surface fatigue is described. Wear fatigue spalling can be seen in the later stages of pitting, which is the first sign of surface fatigue from the contact parts. Spalling typically impacts the opposing parts, like the hub, on both of the connection surfaces. Similar failures also occur on other components known as spur gear, worm and other other contact surfaces. Generally, Some causes of spalling are prolonged stress from excessive load applications, or the components operating with no lubricant or a lubricant that does not meet the correct specification. It can also occur when components are operated beyond the maximum mileage range.

2.6 Surface Contact analytical methods for the splined meshes

The analytical method is one of the best ways to analyze the loading conditions that are acting on the surface externally. This also enables us to understand what the components may fail with those applied moments on them.

The semi-analytical model load distribution for the involute splined shaft was studied by Hong, Talbot, and Kahraman [10]. This method was used to find the other terms of the series of given initial conditions for the problem being considered and proposed by extending the formulations of elastic bodies in contact. The study looked at the four key deformation components of a spline tooth: consisting of tooth bending and shear, tooth base flexibility, tooth contact, and torsional deformations. This model allows the input of arbitrary loading components and arbitrary initial separations. The load distribution properties of splines were determined using this method under various combined loading circumstances.

Felix Muller et al. [20], examined the analytical method applied by selecting both internal and external B-spline contact tooth that is potential zone, in which the zone is discretized into various elements. Also, the effects of design variations and manufacturing errors can be quantified in these discretized elements. In addition, maximum contact stresses in both cases at different torque levels are also close to each other. As a result, all the splined teeth have the same contact stress distribution, which is biased towards the side where the torque is applied, according to both semi-analytical and deformable-body solutions.

Engel B. et al. [15] deals with the strength of assessment of the material by using

ASME and determining stresses. They used a standard known as B106.1M-1985 for a machine shaft design, and it assumes that the shafts are commonly used with fully reversed bending and constant torque (loading conditions). Even though this method is an approximation, it provides a sufficient estimate to check the overall shaft situation. The shaft in this study is chained to a hydraulic cylinder, and they used the maximum hydraulic cylinder force of 25784.6 N. They considered the shaft shoulder where the chain is mounted to be 64.8 mm in diameter. As considerations, five points on the shaft are considered in the force analysis step. These are called the needle bearing position, chain position, first ball bearing position, second ball bearing position, and key position. To draw the stress-cycle diagram (S-N) and to determine the fatigue strength, correction factor, and fatigue life sustained by the shaft before the fatigue damage.

Based on standards the designing and manufacturing process of the splined shaft and the making of the holes or internal pits were considered to have been carried out as cited in [1]. They demonstrate that the geometric establishment, design to manufacturing, and development of spline fitting were studied more. In this study, many of the connection possibilities were studied to the utilization of different constructions. Thus, the manufacturing of the splined shaft and the making splined hole were analyzed by three various manufacturing technologies were analyzed (i.e., milling, grinding, and slotting). As a result, the technological parameters of the splined shaft were investigated analytically based on ASME standards. In this study, the smoothness of the surfaces is not well considered during the process of employing surface finishing factors when that component meets with the internal and external splined gear teeth each other.

2.7 Surface contact stresses and deflections of the splined shaft

Stensland and Anton [13], stated that the flank loads due to the mating of two splined gears to each other, the splined tooth which is an external one is met with an internal which is called a splined hub at the mating face of the parts, the contact stress has occurred between them, this stress may lead to overall failures under varying torques or flank loads. The splined teeth and other gear teeth have been modeled with several different methods. This study looked at a few different ways of determining stress and deflection in teeth. The majority of this work is applied directly to splined gear teeth. Since splines are essentially gear teeth, the methods used to determine tooth deflections and stresses were employed. Much work has also been done with finite element analysis of splines. Spline analysis is simplified because the point

of contact does not change as it does in gear teeth.

Stadtfeld and Hermann J [18], proposed that the spline teeth usually do not fail by bending as gear teeth do. This is because standard spline teeth have short cross-sections and form a very strong beam. As a result, the splined teeth analyzed in this research are more similar to gear teeth because they utilize lower pressure angles, causing them to have longer cross-sections.

Sánchez Miryam et.al [21], this study enhanced the strength calculations of internal spur gear mating due to sharing loads among contacting paths on bending and pitting stresses. the meshing stiffness values from the contacting paths and the values have been Calculated at any point, while the considerable points such were bending, shear, and Hertz's contact stress. The meshing stiffness was expressed by employing inmate accurate equation, as a function of the effective contact ratio exclusively, allowing to express the load at each couple of teeth in a closed-form. The nominal values of the bending and pitting stresses throughout the contact path, as well as their related determinant load conditions on the surface of the splined tooth, were estimated accordingly.

2.8 Finite Element Analysis of the splined shaft

Finite element analysis is a mathematical method for modeling the stresses on an engineering design structure. Structure analysis, fluid dynamics, and heat transfer are all examples of this. The significance of Finite Element Analysis (FEA) lies in its ability to take a complex design and provide insight into its efficiency and robustness. Hong. J, et.al [10], this study proposed a multi-step discretization solution scheme for the examination of semi-analytical loading conditions that were cited to enhance numerical efficiency and reduce CPU time to an acceptable level. The studies on deformable-body of the involute splined shaft teeth with discretization techniques. This techniques approach gets a refined global spline load distribution in numerous steps rather than solving for global spline load distributions directly. Analyzed by using one of the three steps. The first one is defining very coarse contact grids over probable contact zones, the solution of which provides coarse spline load distributions, the setting of a governing equation to those coarse grids meshed on the first step mentioned has been taken into account as a second step, and lastly refining the contact grids along the profile direction. Finally, all of the individual spline load distributions are combined to generate a revised overall spline load distribution.

Francesca Cura et.al [3], this study determines the fatigue life of internal crowned spline coupling failures due to fatigue damage, were at contact pints with the exter-

nally splined shaft. Thus, the finite element method such as Abacus Software is used to calculate contact pressure, teeth sliding, and stress state of an involute crowned teeth spline coupling. To simulate the component, they used only single material, called 42CrMo4. The number of teeth, the modulus, the pressure angle, the mean radius of the splined shaft, the length width, the tooth contact height, curvatures for the shaft and hub, respectively, and minimum curvatures for the shaft and hub are considered as geometrical parameters of the crowned spline coupling. The ANSYS program was used for analysis to cross-check the calculated stress values analytically. The results are investigated by varying the element size from 2 mm to 0.15 mm and applying the torques from 200 Nm to 700 Nm. The mechanical properties for the selected material are poison's ratio is 0.3, and young's modulus of elasticity is 210 GPa. With the use of these parameters, the effects of the evaluation revealed that most contact stress values are considerably greater than those calculated through theoretical models.

Hong J, et.al [11] develops the computational model of the combined finite element and surface integral contact analysis for the gear-shaft splines under three loading cases such as combined torsion, radial forces, and titling moments to normal and helical splined tooth respectively, but in the study, the titling conditions considered for the helical profiles only. They established also nominal load distribution conditions under pure torsion and splined tooth loading conditions (i.e., torsional and radial forces). The modeling was designed based on ANSI Standard B92.1, and the analysis was done by Ansys packages under pure torsion which from ranges 2000 Nm to 4000 Nm. As a result, the load concentration was observed on spline keyways having larger indexing error, this also had smaller clearance, they will engage first. To summarize, the keyways with smaller indexing errors have larger clearances, and they will gradually come into contact when the torque increases to a certain level.

Engel B. et.al [15]. This study demonstrates that the failure modes of the rotary draw bending machine's splined shaft were investigated. The primary goal of the study is to conduct failure analysis on a splined shaft from an obsolete rotary draw bending machine to prevent failure in the second life utilization and to improve the machine's performance. In this study, the analytical method is performed to determine stress and deflection analysis on the shaft when it is subjected to combined torsion and bending loads. The results of the analytical method one were compared to one of the finite element analysis methods. The study included four steps for shaft failure analysis and fatigue life estimation. First, material analysis and hardness tests were performed to determine the type and strength of the material used to make the

shaft. Secondly, an optical examination and surface roughness measurements were performed on the shaft surface. Thirdly, using Abacus software to determine the loads, stresses, maximum linear deflection, and maximum angular deflection were calculated and compared to the values obtained from the analytical method. Finally, fatigue life was estimated using a calculated stress-cycle diagram.

Cui and Minchao [17], the study proposed an integration-rolling extrusion process for the manufacture of the splined shaft, and a simplified sector blank was established with a finite element model to simulate the manufacturing process of it. The plastic forming mechanisms were clearly defined after the results of finite element simulation results. They studied a stress-cycle (S-N) diagram to estimate the theoretical fatigue strength, correction factors, and fatigue life sustained by the shaft before it is damaged. Thus, it can be seen that the shaft can be used in its second life, but it requires some surface treatments to improve reliability and fatigue life. In summary, it can be seen that the shaft can be used in its second life, but it requires some surface treatments to improve reliability and fatigue life. In the simulation, the equivalent stress, deformation degree, and material flow behavior were analyzed in to prevent when operating conditions. From those parameters, the output of the results shows that there is no effective stress distribution, deformation degree, and material flow behavior.

2.9 Splined shaft fracture analysis mechanisms

Various studies were performed to study the failure of the splined shaft under such analytical methods as finite element analysis and experimental work to analyze the problems, which can all be used to determine the failure modes of the splined shaft keyways. The micro-pitting, pitting, cracks, and other failures that act on the splined shaft keyways are of a fatigue nature and were initiated by the torque variations, according to an analysis of the surface flank fracture of the splined shaft [22].

As studied by Yang Yu. et al. [23], the appearance of thermal micro-cracks at the bottom of the spline slots was caused by hardening and subsequent tempering. It is worth noting that the crack has a relatively smooth surface, which is unusual for cyclic loading with sufficiently large torque. This indicates that failure occurred as a result of the crack reaching its maximum length.

Lyashuk et al. [19] are dedicated to increasing the durability of technological equipment elements, resource forecasting, and diagnostics of technical system failures. The basic regularities are examined, and the causes of the extrudes working body shaft failure are identified. The stress-strain state of the contact surfaces of the keyhole of

the extrudes shaft is calculated using the three-dimensional finite element modeling method for torque values of 40.74 Nm to 64.37 Nm and of the extrudes working body shaft. The maximum values of the stress intensity int (max) that occur on the key groove's edge are calculated. They discovered that increasing the distance between the key groove and the fillet of the working body shaft by 2 mm reduces the maximum stress on the edge of the key groove by 15.72 percent. The study considered two crack initiation causes as primary factors, such as the accumulation of dislocations and the cleavage of secondary phases, particularly in the vicinity of the concentrate and unloading adjacent areas, which necessitated concentrate geometry optimizations.

2.10 Experimental works at the flank surface of the splined shaft

To ensure any job, experimental work is very important, and various experimental work is done on the system's splined shaft failures. With advances in science and technology, numerous researchers and designs have been developed to prevent the catastrophic failure of spline shafts. As cited in [24], the numerous machining processes are performed at a wide range of speeds and power in traditional machining processes using lathe machines. To achieve this wide range of speeds the normality of the spline shaft plays an important role in transmitting power from one source to another to obtain the desired machined component. Furthermore, spline shaft design has been improved using experimental and computational approaches, and the implementation of various materials such as alloyed and composite materials as spline shafts has been studied [12, 13].

N. yu Ben et.al [25], demonstrates that the axial cold forging process is suitable for long shafts and has high efficiency as an effective method of forming spline shafts. In the experiments, the two defects of folds and accumulation were found to result in a high forming force and low product quality. To investigate the root cause of the defects, a finite element model with a strain rate-dependent material model was created, with the parameters determined by material testing. In the study, the metal flow was divided into three distinct parts, and relevant parameters to quantify them were proposed. Metal flow, tooth profile, and axial force differences were compared between conventional axial forging, assembling dies, and the new die. When compared to conventional axial forging, the three-die assembly method reduced force by 31.2 percent. Based on the optimization of the assembly method, the die with variable tooth shape reduced the load by 55 percent when compared to conventional axial forging.

Nitish Kumar et.al [7], state that the simulations were run with a standard transmission scheme consisting of two shafts connected by a spline coupling and supported

by four roller bearings (two for each shaft) mounted in an static configuration. The influence of spline coupling teeth micro geometry, as well as the misalignment angle magnitude and torque level, on tooth contact pressure, has been evaluated, as tilting moment is primarily driven by the contact pressure distribution among engaging teeth and the position of maximum stress distribution along with teeth in the axial direction. They conclude that the findings of this study are useful to designers as they suggest some basic criteria for reducing bearing overload, allowing for the design of more reliable and efficient machines because the spline joints use multiple contact surfaces to transmit torque from shafts to rotors. As a result, the mechanical system of the joint is undetermined, i.e., the number of contact points exceeds the number of restricted degrees of freedom.

Cui and Minchao [17], the study proposed that experiments be carried out on specialized forming equipment to verify the finite element model. They used the core region of the blank, so there was almost no effective stress distribution, deformation degree, or material flow behavior. Next, the results are measured and compared with finite element results. The finite element results show good agreement with experiments; thus, the finite element analysis of the integration rolling-extrusion process is credible. In addition, the measurement results show that the dimensions meet the requirements of the heavy truck application. The finding results indicates that the integration-rolling-extrusion process is feasible for the manufacture of splined shafts, especially for surface finishing. However, the surface quality of the formed involute spline shaft is not satisfactory.

Benatar et.al [35], they investigates the gear loading loading conditions with help photo elasticity setup techniques. And also, they develop different gauges for different pressure angles and rotational angles, and etc. In this study, the finite element method is used to find the load distribution along the length of spline, for analysis a frictional contact with 0.15 coefficient of friction and augmented langrage method is used. Entry, midpoint, and exit are the three places that make up the load distribution. The experimental results demonstrate the cyclic nature of the loads and resulting stresses on the spline teeth brought on by the rotation of the spline teeth with respect to the splined gear mesh that loads the splined joint. The tests used photo elasticity to apply various gauges namely, gauges one through five with various pressure angles to various applied torques (loading conditions). The results of the experiments can be repeated with the same test apparatus, test conditions, and test specimens. Of those gauges, gauge three, which measures pressure angle at 30 degrees, is most relevant to the current investigation. Thus, from this investigation, all gauge 3 values are

considered to this study.

2.11 Fatigue failure life analysis of the splined shaft

Fatigue failure analysis investigates material and/or component failure to determine the root cause of cyclic load performance under real-world operating conditions. Material identification is an important aspect of fatigue failure analysis. L. Gang and S. Yong [27] deal with shaft system fatigue life calculation using bend-torsion coupling, the fatigue life of the shaft system decreases as the ship's propulsion power increases and the distance between the two adjacent bearings increases. The study of the fatigue life of a ship's propulsion shaft system has important theoretical implications as well as practical engineering application value for ship design. Based on the ANSYS Workbench platform, the study creates a physical model of the bending and torsion coupling, obtains the transient analysis result at the working speed, and imports it into ANSYS Ncode for fatigue analysis with flexural and torsional coupling. Joe Mattingly et.al [28] Torque transmission between a shaft and a driven member necessitates the use of a key way or integral splined shafts. Due to the close center distance of operation between the two working shafts, co-rotating twin-screw extrudes are designed with extreme engineering requirements. They used a mathematical and FEM analysis of involute and continua spline applications on thin-walled torque transmitting components to predict a significant decrease in the stress concentration factor for continua splines (based on the cycloidal displacement curve). Physical testing confirms that reducing stress concentration results in a significant increase in torque transmission capability in thin-walled torque transmission components.

2.12 Summary of Literature

According to the reviewed literature the summarized one is as follows:

- The splined shaft is affected (failed) by various surface conditions, such as: corrosion effects (due to lack of lubrication), tooth breakage effects (due to high loading conditions), and root failure causes (due to implication of surface contacting stresses). These all are plays major role to start the surface cracking, initial pitting or galling formation on the flank faces of the component.

- Some studies design the model without according to the standard instructions, which could result in further mistakes (such as called misalignment with internal splines or coupling of it) and leads to fatigue failures.

- The studies also showed that the default material characteristics affect the spliced shaft contact region to detect the fatigue life of it, this should be added to fatigue strength factors but didn't consider.

- Also, most researchers used finite element analysis to predict the load applied affect conditions on the splined surfaces and all the slots are carried out to analyze than experimental works because when the shaft is assembled there are no detected parts throughout.

- The analytical modeling of the spline hub and spline shaft has received a lot of attention. Some have recently demonstrated these models using finite element analyses or experimental data, such as those from photo-elastic experiments.

- The phenomenon of successive engagement of spline meshes based on key-way mistakes has been noted by many. As a result of misalignment, load, and changes, several studies also discovered differences in surface loads and related stresses. The development of models that appropriately assess engagement based on current or statistical variances from various error sources hasn't been done much, nevertheless.

2.13 Gap of the research

Through studying all the aforementioned articles in the literature review and closely collecting all the causes of failure from the local garage for confirmation, this study was proposed. Thus, some of the gaps are listed below. These are taken from the literature.

- The majority of the study takes a failed spline analysis into account, as noted in the literature review. When surface pitting has occurred to some extent, the component won't provide the needed services since there aren't adequate goods and services.

- Splines were not considered as a cause of surface finish factors before applying a load factor to it to determine the fatigue life cycle of the process.

- Most studies use fewer splines and their studies focus only on those slots, which surely will not lead to knowing the rest of the key-way surface's effect on their fatigue life. Thus, for each face of keyways as a contact region, surface factors must be considered.

3. MATERIALS AND METHODS

3.1 Introduction

This chapter covers a variety of topics, including the geometry of splined shafts, general contact considerations, surface fitting processes, and analytical and numerical approaches to contact stress resolution. The chart below shows the general approaches used in this investigation.
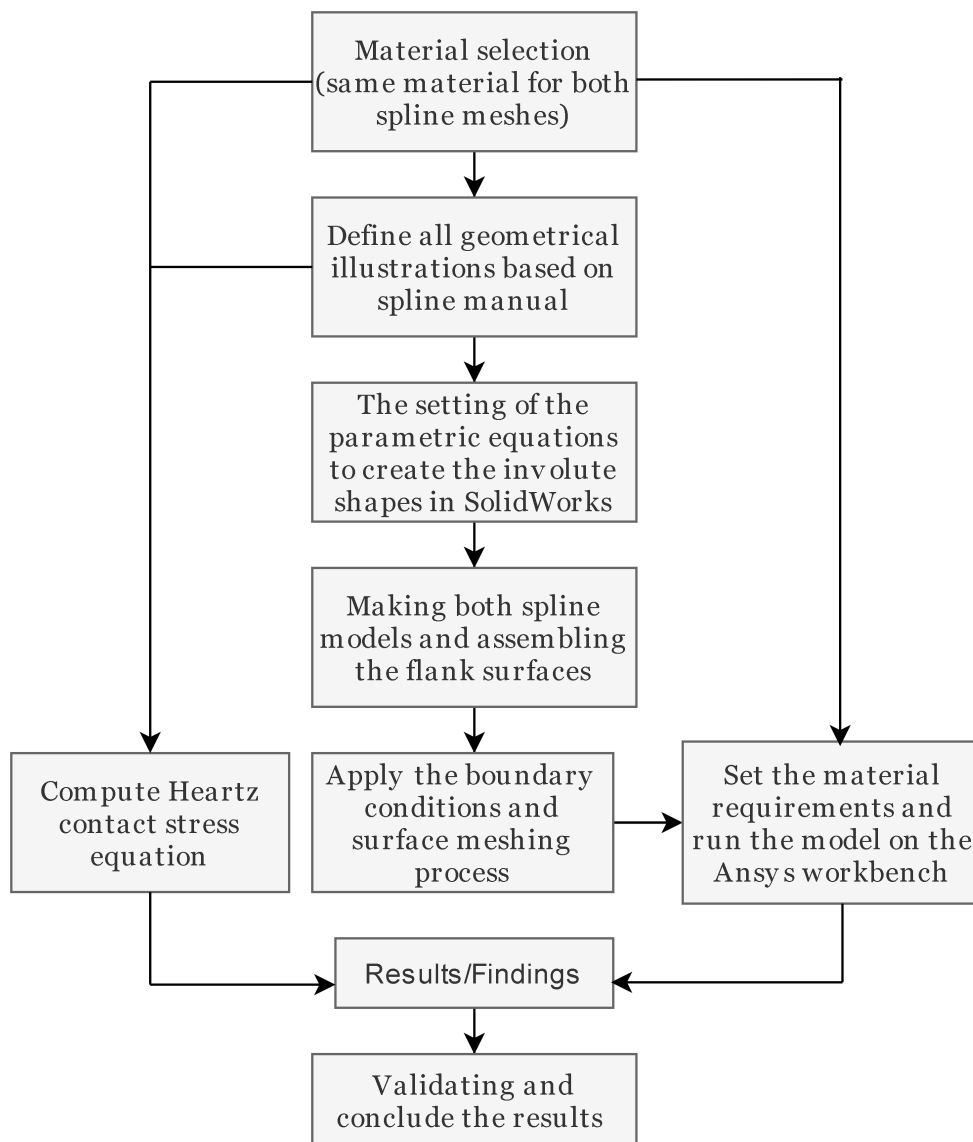
Figure 3.1: Overall methodology flow chart

3.2 The material used for Splined meshes

The driveshaft is one of the major components in the automobile that delivers smooth power from the engine to the rear wheels with the help of an involute spline keyway contact mechanism. Any material used in real-world applications has mechanical properties. The fatigue of such material results from changes in the structure and properties of the material caused by the gradual accumulation of harm under the act of alternating stresses.

The contact surface effect of material sometimes goes through the surface nucleation and growth of cracks, eventually ending up in the quantity of fracture. Such development within the fabric of elements operating underneath contact load is usually due to surface failures and wear.

The ultimate manifested style of cracks, initiated from totally different sites of contact components, once propagated till a piece of material detaches itself, can form a pit or spall, whereas from the purpose of small view, the damage is the accumulation method of pit or fragment of asperities of contact surface due to contact load. Thus, the splined shaft is made using different manufacturing methods. Such surface manufacturing process should be strong and challenging to resist external loads because high torque is transmitted through it.

As mentioned in the literature review presented in Chapter Two, the majority of published studies on the load distribution of splined meshes focused on pure torsional loading; a spline key-ways surface pitting by applying a moment on internally and externally splined faces for a default material. Structural steel (AISI 4130 NS) is one of the default materials for the involute splined meshes. It has high rigidity and a high strength-to-weight ratio, shown in Table 3.1below.

Table 3.1: Type of the splined shaft material and its properties [3, 29]

Type of the material: Structural steel (AISI 4130 NS)			
Mechanical properties of the material	Symbols	Values	Unit
Young's modulus of elasticity	E	205	GPa
Density	ρ	7850	kg/m^3
Yield strength	σ_y	460	MPa
Poisson's ratio	ν	0.3	-
Bulk modulus	B	171.6	GPa
shear modulus	G	80	GPa

3.3 The Involute splined shaft definitions and terminologies

The definitions are detailed below, given by the existing standard on the involute splined shaft, and which were inspected on ANSI B92.1 [9]. As mentioned above and also in Chapter One, Section 1.1, the pitch circle of the shaft is used as the reference circle from which all circular splined shaft dimensions are constructed. The pitch circles of a pair of mating involute splines are equal. All those listed below definition terminologies are derived from the standard manuals of ANSI and all of them are not addressed to the model of the involute shape of the splined shaft [29].

Numbers of spline (N): The number of internal and external involute spline is equal, and they meet at the same time. The height of the spline tooth is much shorter and stiffer than in other gearing systems.

Stub Pitch (Ps): The radial distance between the pitch circle and the major circle of the external spline and between the pitch circle and the minor circle of the internal spline is known as the stub pitch.

Pitch Circle (P): It is also called the diametrical pitch of the circle, which is determined as the ratio of the number of teeth to the diametrical pitch. The point at which the profile and the circle meet each other is known as the pitch point.

Spline Pitch (P/Ps): The spline proportions are indicated by a combination number of one to two ratios; the upper or first number is the diametrical pitch; the lower or second number is the stub pitch.

Major Circle (Do): The circle formed by the innermost surface of the spine. It is the outside circle of the external spline or the root circle of the internal spline.

Minor Circle (Di): The circle formed by the inner-most surface of the spline. It is the root circle of the external spline or the inside circle of the internal spline.

Base circle diameter (Db): The circle from which involute spline shaft profiles are constructed as a major. It is also known as root circle diameter for the involute shape.

Pressure Angle (ϕ): Is the angle between a line tangent to an involute and radial line through the point of tangency. Unless otherwise specified, it is the standard pressure angle. For the application of high transmitting power degrees between 30, 37.5, and 45 degrees are available. An angle of 30 degrees is selected for this work.

Effective space width (Sv): The effective space width of an internal spline is equal to the circular tooth thickness on the pitch circle of an imaginary perfect external spline that would fit the internal spline without looseness or considering the engagement of the entire axial length of the spline. Its also known as the length of the splined shaft which is fitted with hub one.

Actual key thickness (t): The circular thickness on the pitch circle of any single keyway considering an infinitely thin increment of axial spline length.

Effective slot thickness (tv): The effective slot/keyways thickness of an external spline is equal to the circular space width on the pitch circle of an imaginary perfect internal spline which would fit the external spline without looseness or interference.

Active spline length (La): the length of the spline which contacts the mating splines. On sliding splines, it exceeds the length of engagement.

Form circle: The circle which defines the deepest points of involute forms control of the keyways profile. This circle along with the tooth tip circle (or the start of the chamfer circle) determines the limits of the tooth profile requiring control.

Form clearance (Cf): The radial depth of involute profile beyond the depth of engagement with the mating part.

It allows for looseness between mating splines and eccentricities between the minor circle (internal), the major circle (external), and their respective pitch circles.

Face width of the spline (b): The axial length of the contact between the mating splines.

3.4 Involute splined shaft basic terminologies

For such an application side fitting mechanisms were mentioned in Figure 3.2 below. Which is mentioned with its side fit splined meshes mechanisms with a small gap in the arrangement and its proportions are mentioned in Appendix-A (see Figure 5.1) for the pressure angles of the spline shaft of 30, 37.5, and 45 degrees. Meanwhile, to design the current model the following parameters are considered from the listed above terminology which is shown in Table 3.2. For the general applications, the the overall interconnection mesh formulae for the involute spline dimensions are defined in Appendix-A.

Table 3.2: Basic American National Standard Involute Splined shaft symbols

Name	Symbol	Name	Symbol
Pitch diameter	P	Number of spline	N
Base diameter	D_b	Diametrical pitch	D_p
Minor diameter (Int spline)	D_i	Pressure angle (standard)	ϕ
Major diameter (Int spline)	D_o	Circular pitch (Pitch circle)	P_c
Minor diameter (ext spline)	$D_r e$	Actual tooth thickness	t
Major diameter (ext spline)	$D_r e$	Face width of spline	b
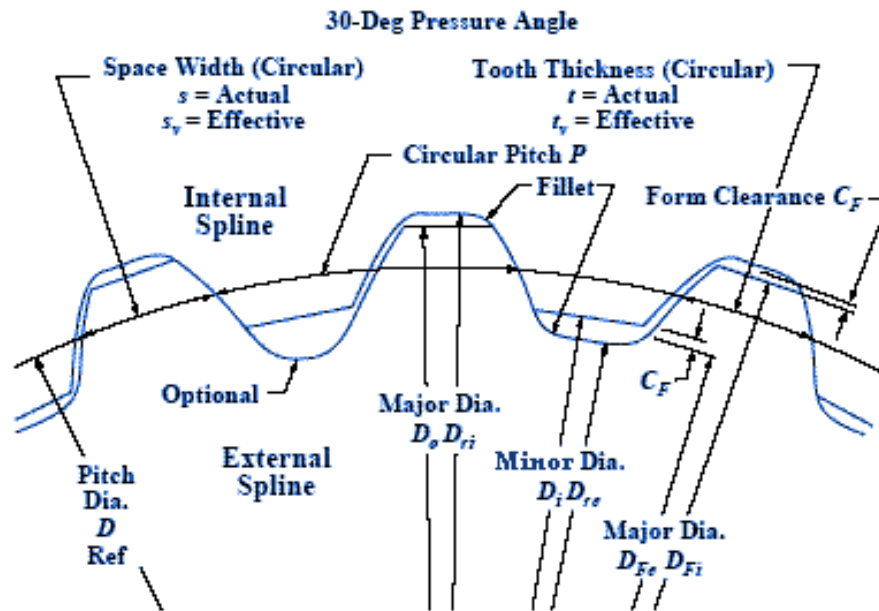
Figure 3.2: Terms for side-to-side fit internal and external splines

3.5 Classes of involute spline shaft fit with its effective clearance

Involute splines must be properly sized and designed to ensure the proper torque capacity and operation. However, this section also details the fits of their characteristics or assembles ways for the different applications by keeping the clearance of all terminologies mentioned in section 3.3. Generally, there are three types of fits covered by ANSI B92.1 [9]. such as minor diameter fit, major diameter, and side fit. Side bearing fit and major diameter fit for a 30-degree pressure angle, and the only type of fit, the side bearing fit for 37.5 and 45-degree pressure angle splines.

Minor diameter fit: As shown in Figure 3.3a, this type of fitting is connected or mates with the top land surface of the component which so-called flank surface of the internal spline. When the operation starts, it leads to the surface fitting of the internal spline.

Major diameter fit: With a minimum amount of location or centralizing effects on the side of the teeth, the major diameter fit offers a minimum effective clearance that will permit contact and location at the major diameter. It shares the same side fit class Figure 3.3b's single space width and tooth thickness tolerance.

Side fit: In this type of fit, the mating members contact only the flank face sides of the key; major and minor diameters of the keyways act as drivers. It is also known as the flank centered position. In this work, this side bearing/fitting mating is considered and it's assembled as shown in Figure 3.3c.

a) minor diameter fit b) major diameter fit c) side bearing fit
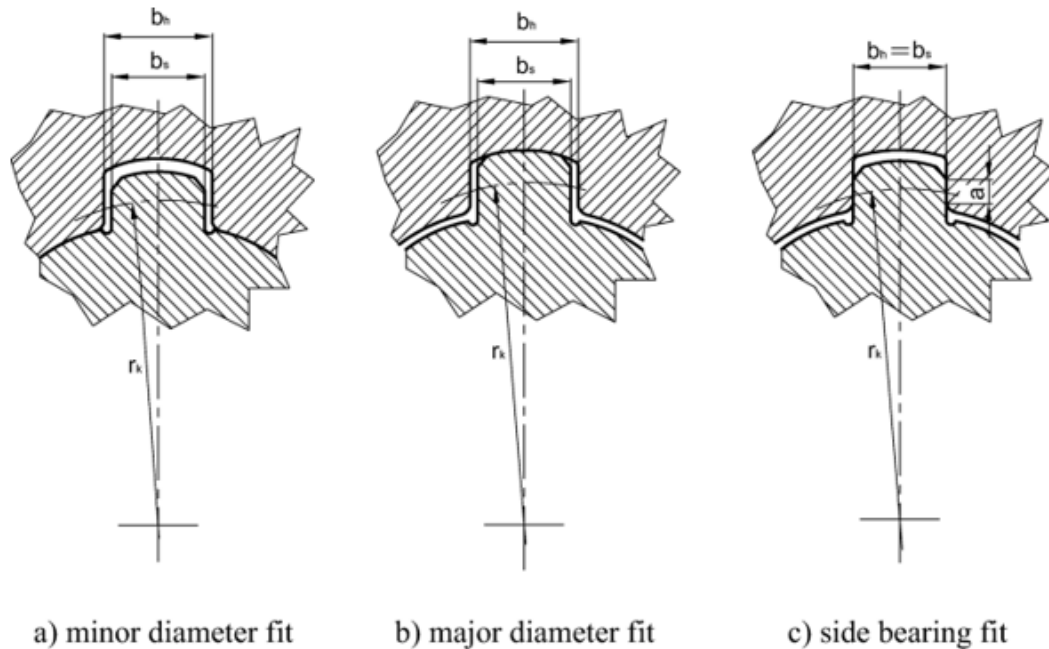
Figure 3.3: Major classes of the involute spline shaft fit [9]

3.6 Involute spline mesh on Solid Works spreadsheets

To draw the spline key-ways of the interconnected dimensions one with another, the solid works were used for this study as the steps of; Solid Works file → Tool → Equation → Sketch entities → Equation driven curve, as mentioned on the Figure 3.4 below.

Figure 3.4: Spec parameters of the involute splined mesh on Solid Works

3.7 Methods to geometrical modeling and involute tooth profile

By applying all the above-mentioned parameters, the interconnected equations are developed on the Solid Works 2020 Premium by considering the number of spline key-ways axially. So, the model of the involute splined shaft developed as shown in Figure 3.5 below. And also, the first two involute curves are generated by the parametric equation for both x and y by considering the radius of the pitch circle, which is also mentioned in chapter one, section 1.11. Generally, the involute curve equation can be given by:

$$x = rx[cos(t) + tsin(t)] \tag{3.1}$$

$$y = rx[sin(t) - tcos(t)] \tag{3.2}$$

Where;

r is the pitch radius of the curve, t is angle parameters in radians, $x(t)$ is a function concerning parameter t and $y(t)$ is a function concerning parameter t
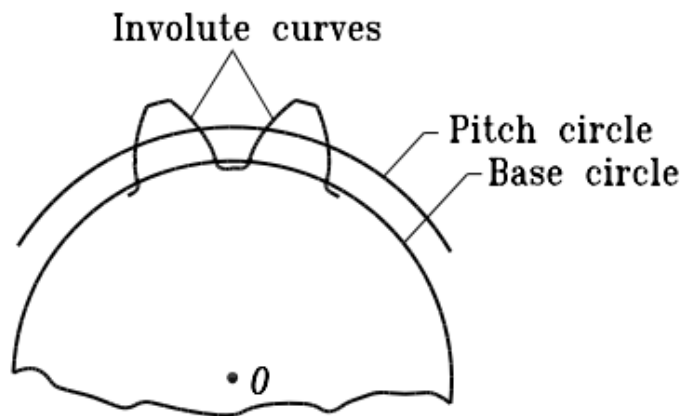
Figure 3.5: Profile generation of involute curve for two branches [30]

By using the above mentioned both Equations 3.1, and 3.2 in the spline equation, a two-dimensional sketch of the involute splined profile will be generated as shown in Figure 3.6 and the side fitting was modelled by keeping root base rule for the lubrication.

By using such dimensional sketch by making it with an equal face of the length, the three-dimensional sketch with the same manner, the internal involute shape of the hub was generated. And also, with the same manner, the internal splined hub will be modelled specifically. The Figure 3.7 shows that magnifying 3d modeling of the spline meshes with effective clearance.

Involute shape generator   External spline shaft   Internal spline hub   Assembled of both
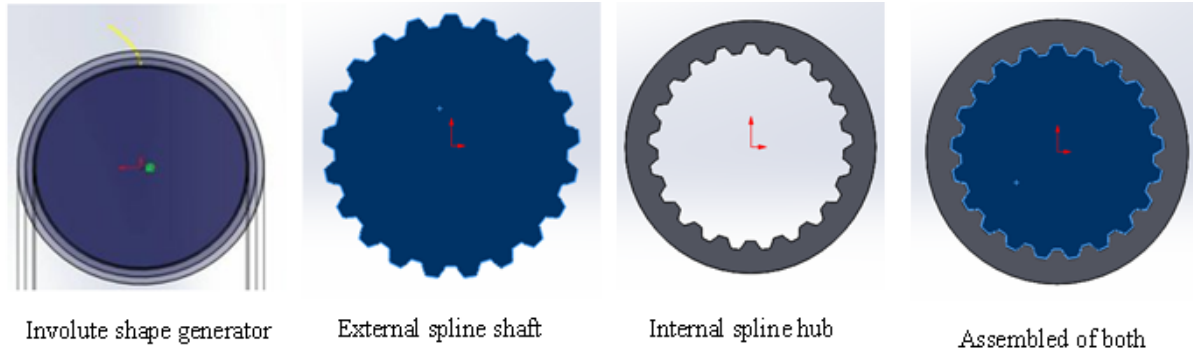
Figure 3.6: Profile generation to making splined shaft meshes
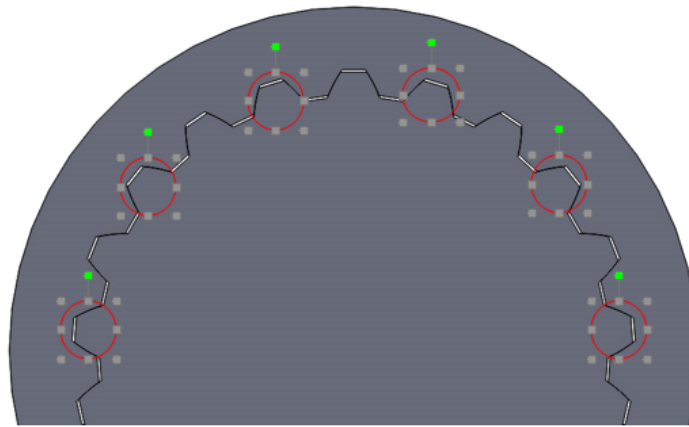
Figure 3.7: Three dimensional side fitting of spline mesh (magnifying)

3.8 Analytical techniques for the flank surface of contact stress

Contact mechanics [26] deals with the deformation of solids that are in contact at one or more points. When two splined keys (hub and shaft) mesh together, the region of contact is theoretically a surface. The curvatures of the individual mating surfaces at the points of contact will vary according to the given dimensions of the splined key-way profile.

At the point where two matching splined surfaces made contact, contact tension developed on the shaft and coupling. The contact region's size is thus determined by the weight and the radius of curvature at the primary contact. The curvature radius of the internal splined hub is negative, but the curvature radius of the external spline is positive as shown in Figure 3.8.

The nature of the meeting of the splined tooth surface contact is, therefore, analogous to that of two contacting cylinders of constantly changing radii of curvature so-called R_e and R_i.
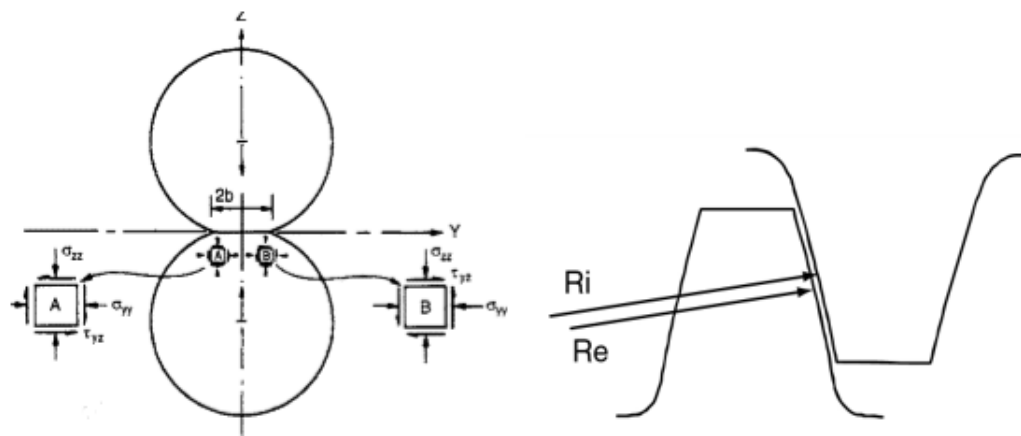
Figure 3.8: Radius of the curvature for both splined meshes [11]

Though theoretically, it is surface contact, the surface develops into a band of certain width along the length of the key-way due to mutual compressive pressure. The stress pattern developed within this band is quite complicated.

According to Dudley [31] when the splined tooth surfaces are in action, a point of maximum compressive stress is created in the center of the hand of contact. The contact stress in both of the meshes is generally the deciding factor for the determination of the required dimensions of spline key-ways.

3.8.1 Hertz contact theories for pressurized surface loading conditions

The well-known German physicist, Heinrich Hertz, developed expressions for the stresses that are created when two curved surfaces are in contact. These surface stresses are universally known as contact stresses or Hertz stresses. This is also valuable for this study as a whole to determine the contact stresses that happened on the splined face or flank of the vehicle.

The theory of contact mechanisms emphasized non-adhesive contact, which may be separated without adhesion forces. Contact issues that satisfy the no-adhesion requirement have been solved using a variety of analytical and numerical methods. Complex forces and moments are transferred between bodies where they make contact, leading to complex contact mechanics issues.

A frame of reference with static items is typically constructed to simplify the solution process. The interface between the internal and external constructed splined meshes is experiencing surface traction interaction. The following presumptions are

established when examining the solutions to Hertz contact problems based on their interactions.

- The strains are small and within the elastic limit and surfaces are frictionless.

- The surfaces are continuous and non-conforming (implying that the area of contact is much smaller than the characteristic dimensions of the contacting bodies).

- Each body can be considered an elastic half-space.

- The applied load, F is uniformly distributed along the entire length of the cylinders.

The fundamental element of classical contact mechanics investigations is the Hertz contact issue, which involves interaction between spheres, cylinders, cones, and flat surfaces [13].

In the study of contact mechanics, the cylinder-on-flat contact arrangement is typically used extensively where the cylinder is thought of as the applied load and the flat surface as the substrate. This section provides a quick review of the Hertz theoretical solutions for the contact pressure and contact area half-width, as shown in 3.9.
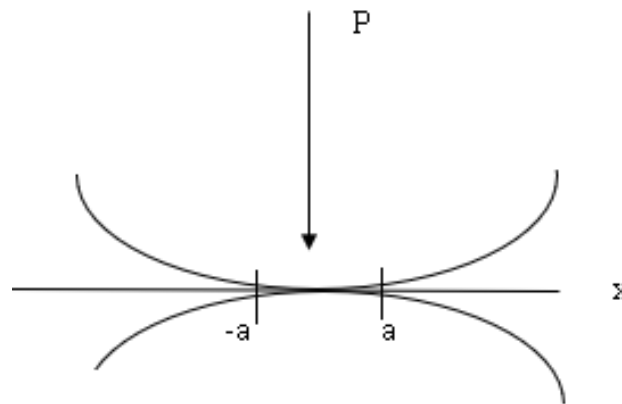
Figure 3.9: Schematic view of the cylinder on flat contact configuration

The definition of the Hertz contact pressure distribution, p(x) [31] is:

$$P(x) = P_o \sqrt{1 - \frac{x^2}{a}} \qquad (3.3)$$

Where; P_o is the maximum contact pressure, a is contact half-width length, x is the position of the cylinder and their relations are given by:

$$P_o = \left(\frac{PE}{\pi R}\right)^{\frac{1}{2}} = \sqrt{\frac{PE}{\pi R}} \tag{3.4}$$

Since, the half-width of the contact area through the length of the cylinder is also given by:-

$$a = \frac{4PR^*}{\pi E^*} \tag{3.5}$$

Where, P is the normal load acting across the contact surfaces, R^* is the relative curvature, and E^* is the equivalent elastic modulus of the contacting bodies. The term of equivalent with Poisson's ratio are also defined by:-

$$R^* = \left(\frac{1}{r_1} + \frac{1}{r_2}\right)^{-1} E^* = \left(\frac{\left(1 - V_1^2\right)}{E_1} + \frac{\left(1 - V_2^2\right)}{E_2}\right)^{-1} \tag{3.6}$$

where;

r_1 and r_2 are the radii of the contacting surfaces, E_1 and E_2 are elastic moduli v_1 and v_2 are the Poisson's ratios of the internal and external splines respectively.

The maximum pressure distributions are specified when both the external and internal splines meet, as shown in Figure 3.10 and numerically mentioned in the chapter four as shown in Figure 4.1.
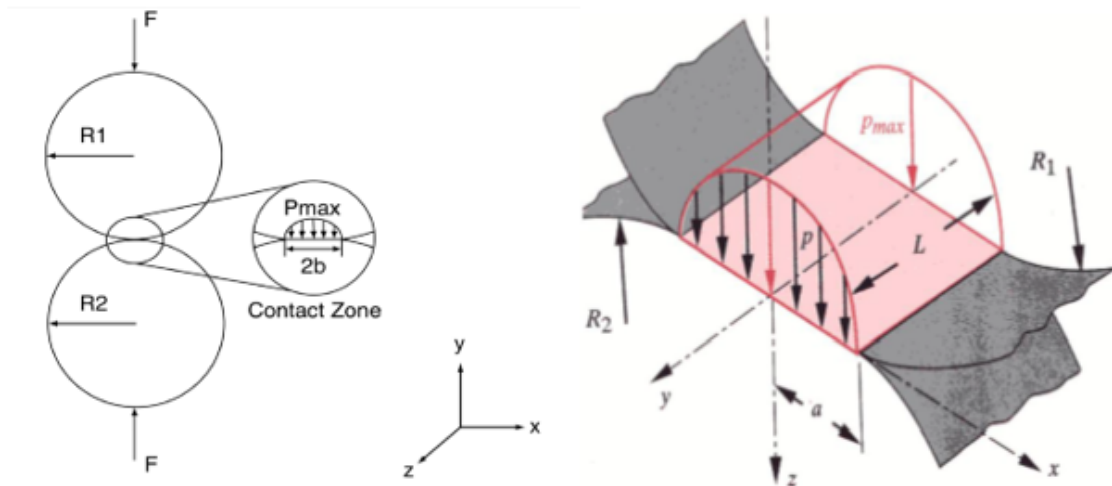
Figure 3.10: Hertz's pressure distribution model for the parallel contact cylinders [13]

Where the pressure is developed in the contact region with an elliptical shape, the re-

gion is measured as 2b as shown in Figure 3.10). Thus, the half-width of that elliptical
shape is given by:

$$b = \sqrt{\frac{2F}{\pi l} \frac{\frac{(1-V_1^2)}{E_1} + \frac{(1-V_2^2)}{E_2}}{\frac{1}{r_1} + \frac{1}{r_2}}} \qquad (3.7)$$

Where;

b is ellipse half-width, F is force acting on the surface of the cylinder, L is length of the
cylinder, r_1 and r_2 are the diameters of the cylinders for external and internal spline
key-ways respectively.

The meshing of two involute splines has similar to the contact between two cylinders
and based on the standard spline manual [9], the Table 3.3 is mentioned as parameters
for the flak surface of it.

Table 3.3: Half-width and hertz contact stress data for the torque of 1350 Nm

Parameters	Symbols	Values	Units
Force applied (moment conversion)	F	45000	N
Poisson's ratio	ν	0.3	-
Modulus of Elasticity	E	205	GPa
Length of the spline	L	38.1072	mm
Internal spline radius	r_1	30	mm
External spline radius (with effective clearance)	r_2	29.9438	mm

Hence the Hertz equation can be used to determine the contact stresses in the mating
spline of the shaft and hub. The Hertz equation for contact stress in the slot of mating
spline shaft and hub is given by,

$$\sigma_c = \sqrt{F \frac{(1 + \frac{r_1}{r_2})}{r_1 b \pi [\frac{1-v_1^2}{E_1} + \frac{1-v_2^2}{E_2}] \sin \phi}} \qquad (3.8)$$

Where;

σ_c is the contact stress in the mating keys of the splined mesh, F is the force acting
on the surface of the cylinder, $r_1 and r_2$ are pitch radii of two connecting faces, b is the
face width of the splined tooth ,Φ is the pressure angle, $v_1 and v_2$ are poison's ratio of
both connecting materials (similar to both slots), and E_1 and E_2 are young's modulus
of elasticity for both of the components.

In this study, the torque is taken into account as surface loading conditions for the range of the engine power of the HOWO dump truck, which is from 1350 Nm to 150 Nm [36].

By using the hertz contact stress equation 3.8 and the results shown in Table 3.3, the variation of surface contact stress is solved as shown on Table 3.4. Such tabular results are compared with numerical results in Chapter Four on Table 4.1.

Table 3.4: Hertz's contact stress for the torque transmission

The moment applied (Nm)	Hertz contact stress (MPa)
1350	2.874
1200	2.710
1050	2.534
900	2.350
750	2.141
600	1.915
450	1.459
300	1.021
150	0.527

3.9 Numerical Analysis for the splined meshes

Finite element analysis for spline-hub connection is carried in ANSYS 19.2 for static pure torsion case and the male and female spline mesh was modeled by Solid-Work 2020. Thus, all the listed terms below (i.e., CONTA identifications, contact types and formulations/algorithms, meshing characteristics, contact sizing, surface mesh refinement, and relative boundary conditions) are addressed under this analysis respectively.

3.9.1 Identification of the Contact and Target (CONTA) surfaces

In ANSYS software package, there are two contact methodology assigning surfaces, which are called target surface and contact surface. The contact and target surfaces form a contact pair. In simple terms, when two separate bodies touch each other, contact and target represent the two bodies. This means that the nodes on the contact surfaces will be prevented from penetrating into the volume of the target surface. To apply the external loading conditions to the flexible and fixed components in such type connections, they must first be identified.

In this study, the splined hub is considered a fixed component and to be a contact

surface, and the splined shaft is considered a flexible or target surface, taking the following conditions into account [37] and as shown in Figure 3.11 and 3.12. That is why this study considered the splined shaft as a contacted surfaces by considering on the following reasons.

- It is subjected to applied forces, rotations and connected to other specific element.

- The motion is adjusted by the equilibrium condition of the engine variable torques.
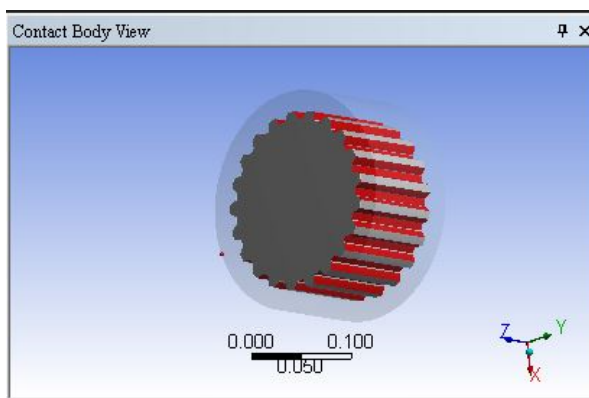
Figure 3.11: Contacted surfaces (shaft)   Figure 3.12: Targeted surfaces (hub)
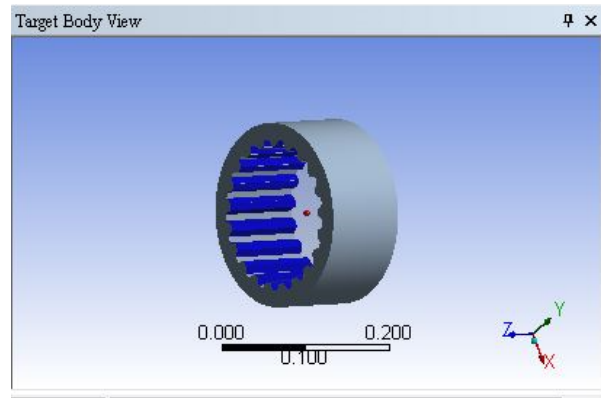
3.9.2 Contact definition for the splined meshes

Contact elements must be defined after giving coupling in ANSYS access to material properties. In ANSYS, contact properties are provided in three steps. It is necessary to define the contact class in the initial phase. Two contact classes typically exist: rigid-flexible and flexible-flexible.

One or more of the contacting surfaces are viewed as rigid in a rigid-flexible contact. Flexible-flexible contact, the more common type, belongs to the other class. In this setting, every contacting body is flexible. There are three available contact behaviors. They are referred to as surface to surface, node to node, and node to surface.

- Point-to-point contact: also called as node to node contact behaviours. They contacts at specific points (node). Typically, only modest quantities of relative sliding deformation between contact surfaces are permitted by these kinds of contact issues. such behaviours leads to stress concentrations.

- Point-to-surface contact: These kinds of contact issues enable considerable distortion and relative sliding. For the point to surface contact, the point is contact and the surface is target.

- Surface-to-surface contact: In this contact behavior, internal and external sur-
faces are equal to the contacting surface. Thus, identifying the contact sur-
face and the target surface is the initial stage in a surface-to-surface interaction.
When one body comes into contact with a surface that is convex but not concave,
the convex surface is chosen as the contact and the concave as the target.

3.9.3 Application of contact algorithm tools for the Numerical Analysis

ANSYS offers five different contact formulations [37]. Contact compatibility can
be satisfied using either the penalty approach or the combined penalty and Lagrange
multiplier factor method. By recommending contact stiffness, the penalty methodol-
ogy ensures approximation compatibility. Through the creation of additional contact
forces that are designated as Lagrange forces, the combined penalty and Lagrange
multiplier factor approaches fulfill compatibility to a user-defined exactness.
However, MPC and Beam are not significant for such contact approaches and are rel-
evant for bound and no separation contact. Only the Augmented Lagrange controller
is used for this study because iterations if penetration is too large, Contact penetration
is present but controlled to some degree and useful for any type of contact behavior
[37] as based on details and relative definitions shown in Table 3.5 below.

Table 3.5: Applications of contact formulation for d/t views on the ANSYS

Effects	Penalty contact	Lagrange contact
Penetration	Allowed/Required	Not allowed
Contact stiffness	Relevant	Irrelevant
Over constraint	Not possible	Possible
Accuracy	Low	High
Computational time	Less	More

3.9.4 Application of boundary conditions for both splined meshes

In FEA, boundary conditions are imposed on the physical domain under investi-
gation to ensure convergence of the solution to acceptable outcomes [23]. An area of a
structure where the external force or displacement are known at the commencement
of the analysis is said to have a boundary condition.
The spline shaft bearing locating surface is used as a friction-less surface, the spline
hub is mounted with fixed support, and the components option is used to apply a
moment to the spline shaft flange, as shown in Figure 3.13 identifications. Thus, the
boundary conditions include Fixed support for splined hub, Moment taken into ac-
count as as surface loading condition, Displacement to indicate the forward direction,

and friction-less support for the splined shaft and the result was done by adding those alternating conditions on the analysis media.
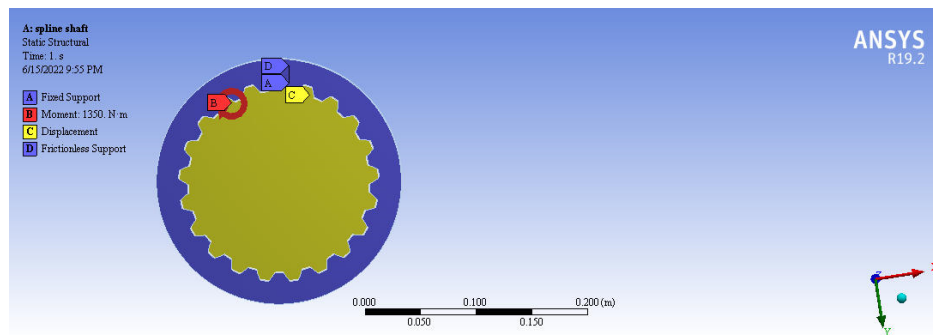
Figure 3.13: The applied boundary conditions on the ANSYS Workbench

3.9.5 The overall meshing processes for the both splined meshes

The mesh influences the accuracy, convergence, and speed of the answer. Furthermore, the time it takes to form and mesh a model is usually a major portion of the time it takes to induce results from a CAE solution. The tetrahedron meshing process with fine mesh is taken into account for the following cases:

In the ANSYS software, numerous ways of meshing solid designs are counseled. Among the types, the Tetrahedron meshing methodology is the most well-liked one, wherever an all-tetrahedral mesh is formed. Because, it is a 3D generalization of a 2D triangular mesh. Tetrahedral elements are commonly constructed as equilateral, such as in systems with circular curvature and for CONTA 170 to CONTA 174 (see more appendix illustration on Figure 5.5).

All the following process, as mentioned in the Figure 3.14 (so-called as the scope of the meshing process) taken in account on this study analysis. Additionally, Following each patch of geometry during the meshing process is referred to as patch conforming. Consequently, patch conforming will provide the highest-quality mesh if the geometry is strong and impenetrable.
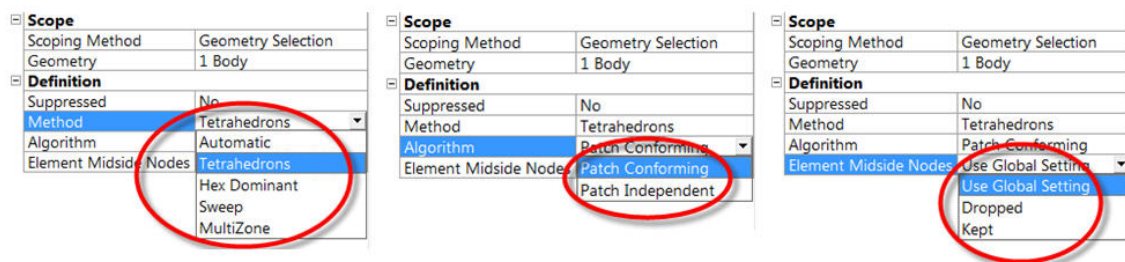
Figure 3.14: Flow process of meshing for both involute splined meshes

3.9.6 Contact surface mesh refinement and contact sizing

In ANSYS, the structural analysis was carried out after importing the assembled model. The both assembled involute spline contacting surface must be defined for the contact algorithm, contact surface refinement, and contact sizing. Though, the Contact and target elements must be referred to as the same characteristics to define a contact pair completely. In the current analysis, the contact elements CONTA174 and Target170 are used detail in Appendix B, on Figure 5.3 and cited in [37] .

Increasing elements at contact elements is possible with ANSYS Workbench. Element densities are described in terms of levels from 1 to 3. One represents the least amount of refinement at the given place, while three represents the most refinement. The elements are created randomly and even go against shape restrictions. Then, a frictional contact algorithm taken into account 0.15, contact sizing which is 3mm and the refinement variation which employed on shown in Figure 3.15 and 3.16.
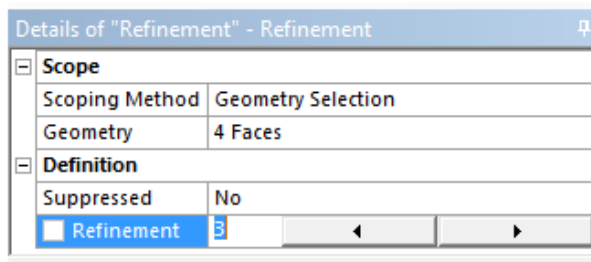
Figure 3.15: Mesh refinement   Figure 3.16: Contact size
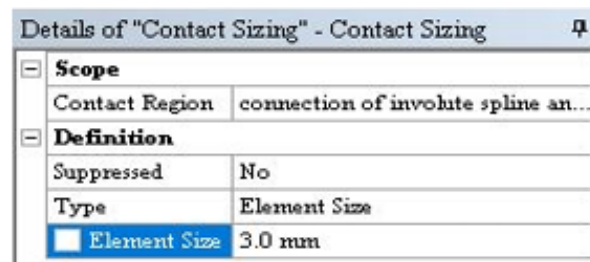
All the above mentioned techniques give such outputs which shown in Figure 3.17.
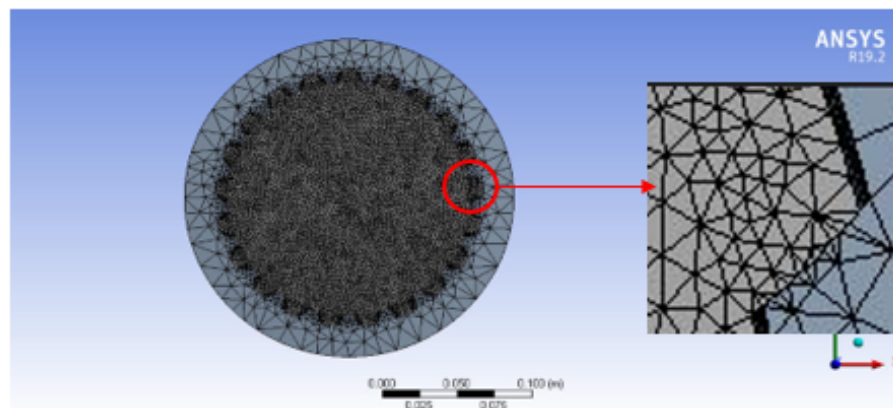
Figure 3.17: Tetrahedron meshed application for both splined assemblies

In order to show briefly, the tabular data, Table 3.6 includes the parameters and all properties which applied on numerical analysis (splined meshing process).

Table 3.6: Meshing characteristics for Finite element Analysis

S.No	Properties	Parameter
1	Element type	Tetrahedral
2	Element sizing	3mm
3	Number of elements	215,923
4	Number of nodes	369,454

3.9.7 Fatigue life estimation outline in the ANSYS Workbench

In order to desired out, the fatigue life was carried by the following two close mechanisms such as Overall work flow process an the ANSYS Workbench and the overall work process from initial modelling to final desired output and all them are mentioned on the following two consecutive figures (Figure 3.18 and Figure 3.19)
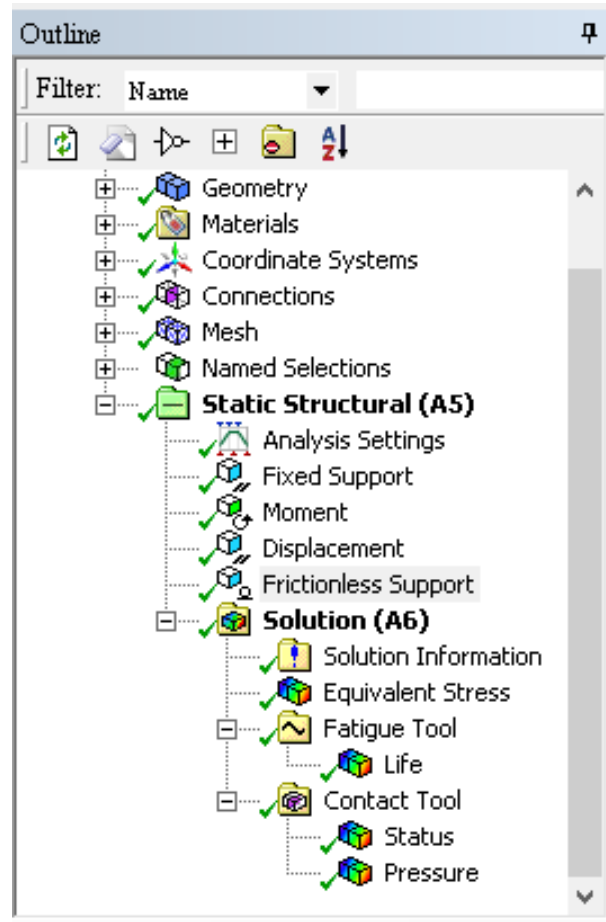
Figure 3.18: Overall work process outline on the ANSYS Workbench

```
┌─────────────────────────┐
│ Draw the solid model by │ ◄───────────┐
│ using Solid Work 2020   │             │
│ based on the involute   │             │
│ spline manual           │             │
└───────────┬─────────────┘             │
            │                           │
            ▼                           │
┌─────────────────────────┐            │
│ Flank faces of the      │ ◄──┐       │
│ splined mesh assembling  │    │       │
└───────────┬─────────────┘    │       │
            │              Not good     │
            ▼                  │        │
       ╱─────────╲             │        │
      ╱ Check     ╲────────────┘        │
      ╲ perfect   ╱                     │
       ╲ involute╱                      │
        ╲spline ╱                       │
     good face assembling               │
       │                                │
       ▼        No, Perfection variation│
┌─────────────────────────┐            │
│ Save the model as IGES  │            │
│ and export to ANSYS     │            │
│ Workbench               │            │
└───────────┬─────────────┘            │
            ▼                           │
┌─────────────────────────┐            │
│ Set the material and    │            │
│ apply its properties    │            │
└───────────┬─────────────┘            │
            ▼                           │
┌─────────────────────────┐            │
│ Apply all the listed    │            │
│ boundary conditions     │            │
└───────────┬─────────────┘            │
            ▼                           │
┌─────────────────────────┐            │
│ Generate meshing        │            │
└───────────┬─────────────┘            │
            ▼                           │
       ╱─────────╲                      │
      ╱ Define    ╲─────────────────────┘
      ╲ contact   ╱
       ╲ area by ╱
        ╲setting╱
     parameters
       │
  Yes, perfect variation
```

Figure 3.19: Overall numerical flowchart for fatigue life estimation

4. RESULTS AND DISCUSSION

4.1 Introduction

One of the most preferable methods for the contact stress for the component of the involute splined shaft is the Finite element method [20]. So, the contact stress is determined in the area of involute face contact of the splined hub and shaft was calculated by using the analytical Hertz contact stress equation, and the finite element analysis was by using ANSYS Workbench 19.2. All the results which presented here are described as based on the flow chart steps that illustrated on the Figure 3.19.

In this chapter, all the plotted graph codes are mentioned where in the appendices and all the analysis was done by considering the listed boundary conditions except fatigue strength factors or surface finishing factors. the surface finishing roughness parameters are also mentioned in Appendix-B1.

4.2 Pressure distribution along the contact area of the splined mesh

The contact stresses for two cylinders are fairly located at each point mentioned in chapter three, Figure 3.10, section 3.3.1. that the three elements of contact stress dissipate considerably to a depth adequate to three times the contact half-width. This is often additionally true for contacting external/internal cylinders of various radii, but the contact is not local.

The load is distributed over the total length of the splined meshes, so the contact stress should be significantly lower as shown in Figure 4.1. For this reason, the contact stress doesn't contribute considerably to the maximum stress at the bottom of the tooth. However, it's important t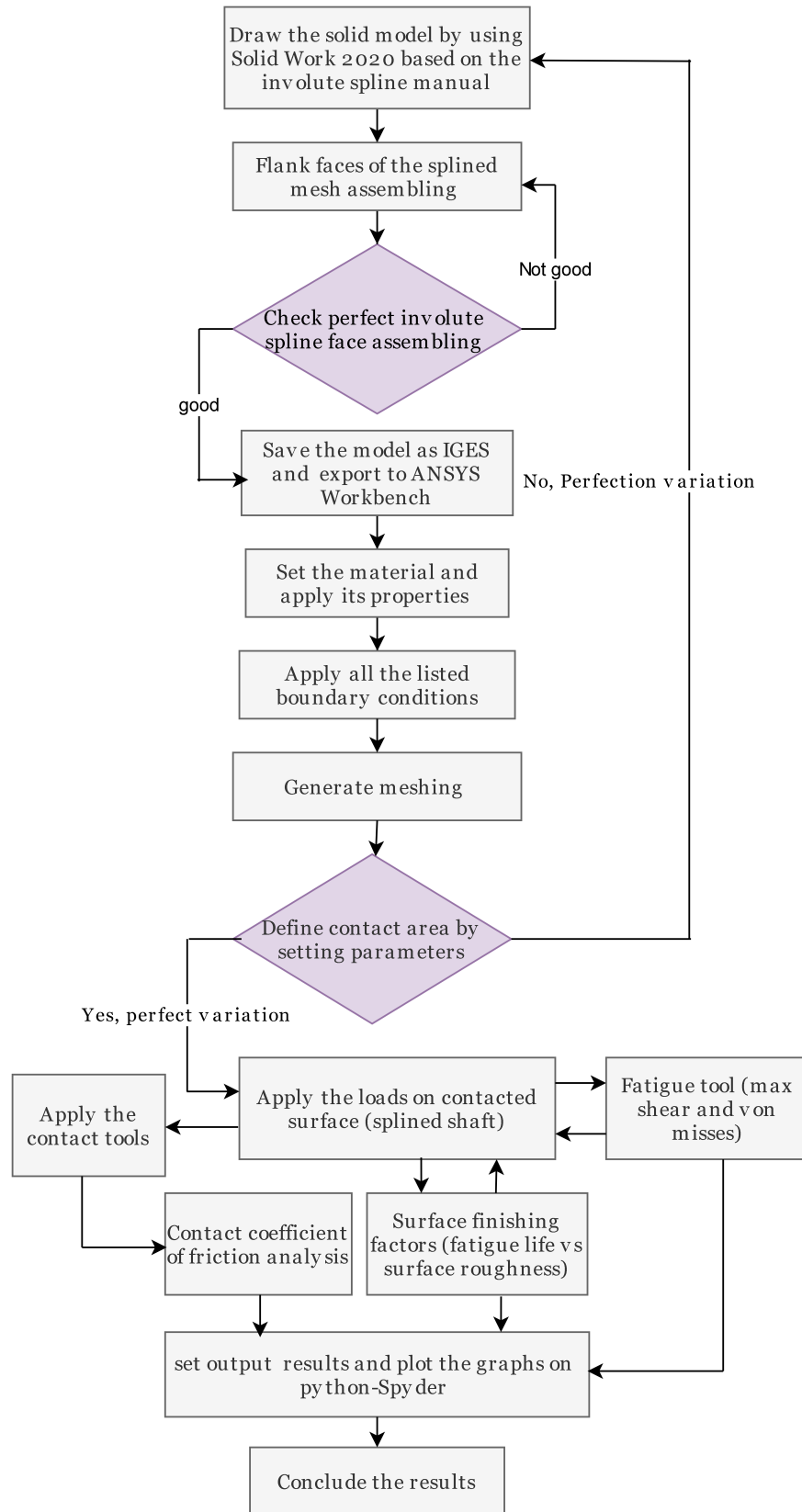o observe the contact stress to avoid surface failure, because the pitting is formed on the surface before any acting on other surfaces. Its easy to detect even to replace the component before going to other surfaces.

The contact pressure variation through to contact area relations is detailed in Figure 4.1. which is analyzed only at a maximum loading conditions moment of 1,350 Nm. When the surface contact area near to zero from either positive and negative direction, the contact pressure will be maximum which leads to the surface pitting. This confirms also that the pressure is inversely proportional to contact area of contact surface. Good validates as shown on analytical variations at the point contact area 0 in Figures 3.18 and 4.1. (And see Appendix-C of Figure 5.5 CAE analysis).
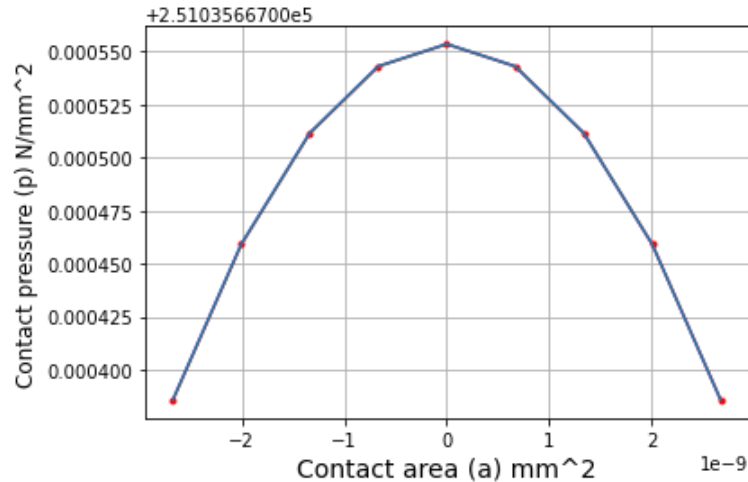
Figure 4.1: Contact pressure profile variations along the contact area

4.3 The Variation of contact stress for different loading conditions

As mentioned in Chapter Three, the contact stresses were considered the moments
(surface loading conditions), which range from 150 Nm to 1350 Nm. It is shown in Table 3.2. When the finite element simulation, the smaller load error between analytical
and numerical methods was considered and validated with experimental investiga-
tions which shown in Table 4.1 below.

The Table leads to another way of determining the stresses because it shows that cor-
rectness means there's less error in both analytical and numerical calculations even in
experimental works. Thus, the entire Numerical data is derived from ANSYS Work-
bench based on contact sizing of 3 mm and a coefficient of friction of 0.15.
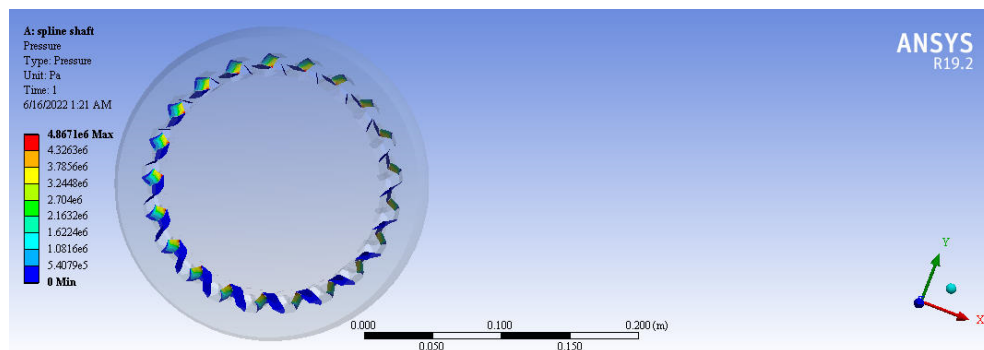
Figure 4.2: Contact stress by FEA for max moment of 1350 Nm

The numerical contact stresses for the minimum value of the moment 150 Nm are
illustrated as shown in the Figure 4.3. It is taken into account as a sample, the result
of the analysis were mentioned on it.
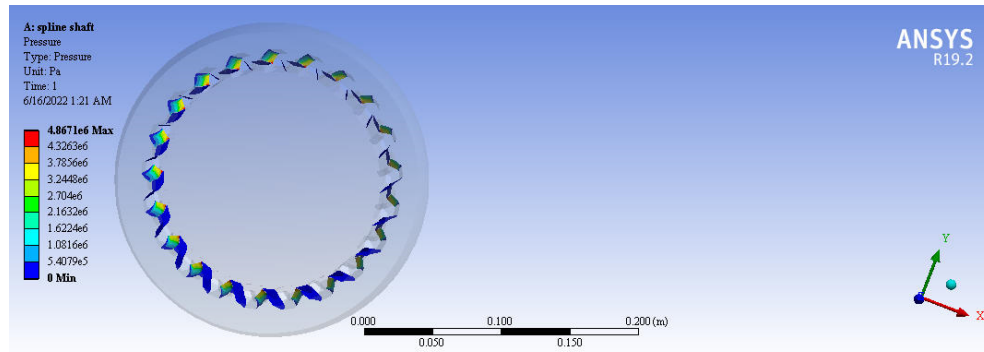
Figure 4.3: Contact stress by FEA for min moment of 150 Nm

The experimental experiments are discussed in Chapter Two, Section 2.7. Thus, all the extracted data are plotted on python-spyder code to analyze the contact stress variations. It has been also used for analysis for all three analyses it is also shown in Appendix G, Figure 5.10 and mentioned in Table 4.1.

When the loading conditions is increased the the surface contact is also increased but its not true for the percentage variations among two of them. The results smoothly agree with three of the analysis and when the surface contact increases directly surface pitting will be started.

Table 4.1: Comparison of contact stress by analytical, num, and expt'l investigation

Moment (Nm)	ANSYS work-bench contact stress (MPa)	Hertz contact stress (MPa)	Photo elasticity (MPa)	percentage Error between A and B	percentage Error between A and C
	A	B	C		
1350	4.867	2.874	2.604	5.90	5.35
1200	4.326	2.710	2.414	6.26	5.58
1050	3.785	2.534	2.278	6.69	6.02
900	3.248	2.350	2.046	7.23	6.30
750	2.704	2.141	1.779	7.92	6.58
600	2.1632	1.915	1.596	8.85	7.38
450	1.6224	1.459	1.289	8.99	7.95
300	1.0816	1.021	0.972	9.44	8.99
150	0.5408	0.527	0.515	9.74	9.52

4.3.1 Percentage error variations due to the surface surface contact stress

The numerical, analytical, and experimental percentage error distribution due to surface loading conditions on surface contact stress are plotted in Figure 4.4 and the code was illustrated on Figure 5.11.

when the percentage error increases relatively the loading conditions (surface load) are decreased, this means the surface contact stress is decreased. on the other-hand, the contact pressure come more and more due to contact area, that have the same concept on mentioned on Figure 4.1.
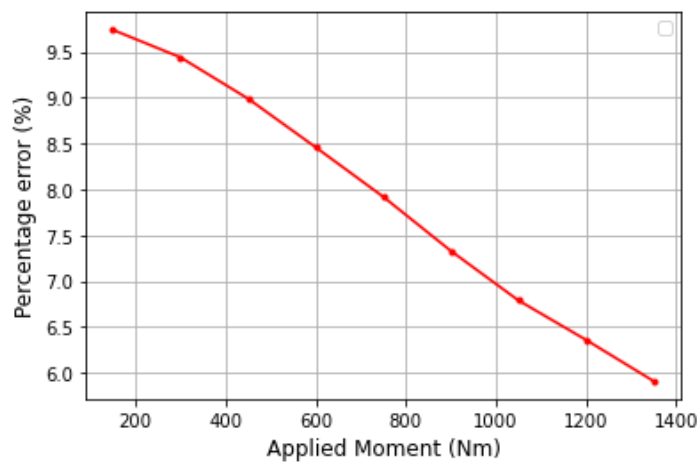
Figure 4.4: Percentage variation of all the three contact stresses

4.4 The effects of coefficient of friction on contacting surfaces

The force due to friction is usually independent of the contact area between the two surfaces. The Maximum contact pressure at maximum and minimum of 0.25 and 0.01 coefficient of friction is shown in Figure 4.6 and Figure 4.5 respectively.
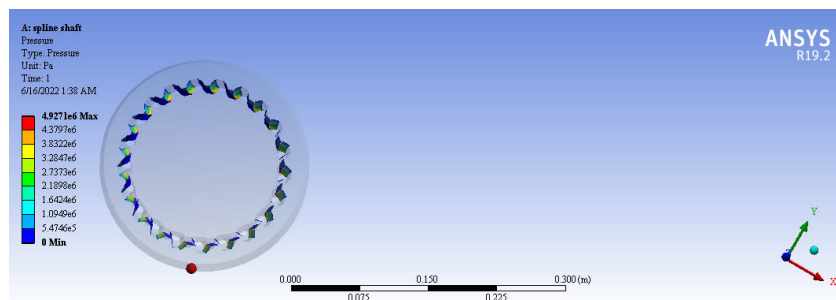
Figure 4.5: Maximum contact pressure at minimum 0.01 coefficient of friction
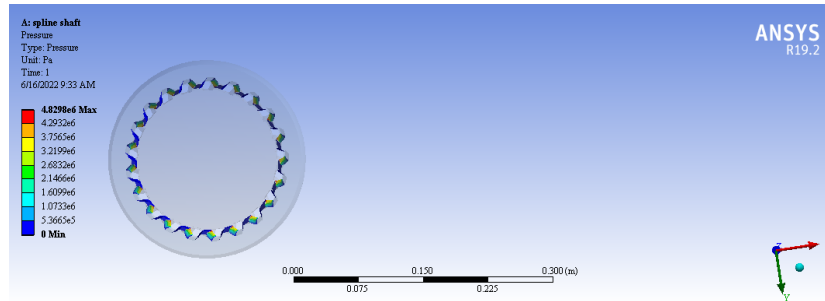
Figure 4.6: Maximum contact pressure at maximum 0.25 coefficient of friction

The FEA results are taken for five different coefficients of friction and for the single maximum surface loading condition at 1350 Nm and mentioned on Table 4.2.

Table 4.2: Different coefficient of friction at maximum loading contact stress

Coefficient of friction (μ)	Maximum contact stress (MPa)
0.01	4.9271
0.05	4.9089
0.15	4.887
0.20	4.867
0.25	4.848

Graphically the tabular Data has plotted in Figure 4.7 and the code for this analysis is mentioned in Appendix-J, Figure 5.11. It shows that the coefficient of friction increases the maximum contact stress is also increased respectively. That means the friction can be lowered by employing a superior surface finish and adding lubricant in the contact area, resulting in less wear and hence longer surface fatigue life.
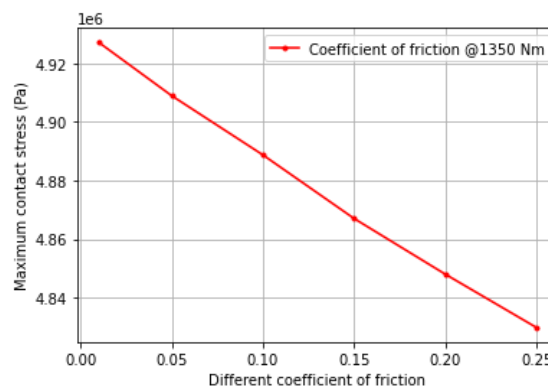
Figure 4.7: Different μ for maximum loading conditions contact stress

As a result, when the coefficients of friction increase, the contact stress also increases

at maximum loading conditions. This variation shows how the surface roughness is
taken into account in order to determine surface finishing parameters due to this the
effects of coefficient of friction results.

4.5 Contact surface finishing modifying factors

Standard tests are conducted to obtain the fatigue strength or endurance limit for
materials. There will be physical differences between the test specimen and the actual
machine part. In order to correct such factors are load factors, temperature factors,
reliability factors, size factors, and surface factors. Among these factors, only the sur-
face factor is considered for this study, depending on the surface machining process
and their surface finish roughness.

The surface condition may be characterized by two factors: notch-like surface irreg-
ularities or roughness; and residual stress within the surface layer. Irregularities on
the surface act as stress concentrations and result in pitting initiation at the surface.
Once the measurement of the surface roughness is understood, Figure 4.8 details an
empirical chart used to confirm the surface finishing modifying issue for steels.

In the contact zone, the compressive stresses and shear stresses within the zone are
the main stresses on the surface. All those parameters are analyzed based on surface
finishing roughness.
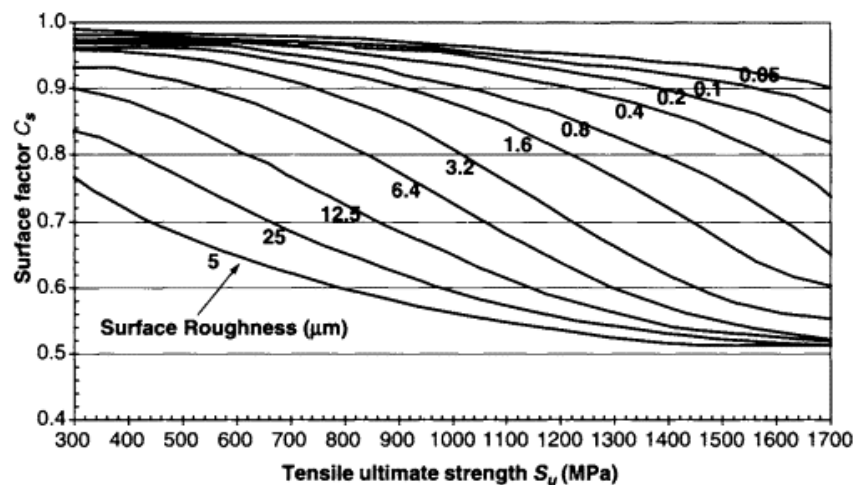
Figure 4.8: Qualitative description of surface finish roughness values [31]

Generally, Surface finish is more critical for high-strength steel and at high-cycle fa-
tigue lives where crack initiation dominates the fatigue life. The effect of surface finish
on fatigue strength is minimal in such cases, according to a study by the US Steel In-
stitute (USSI). With the same manner, the involute splined mesh surfaces are finished

by keeping the information as based on the information of 4.8 and Figure 4.9.

In Figure 4.9, all the mentioned surface finishing processes such as mirror polished, fine ground, machined, and hot rolled are finished by means of surface roughness desired values which are mentioned in the Figure 4.8.
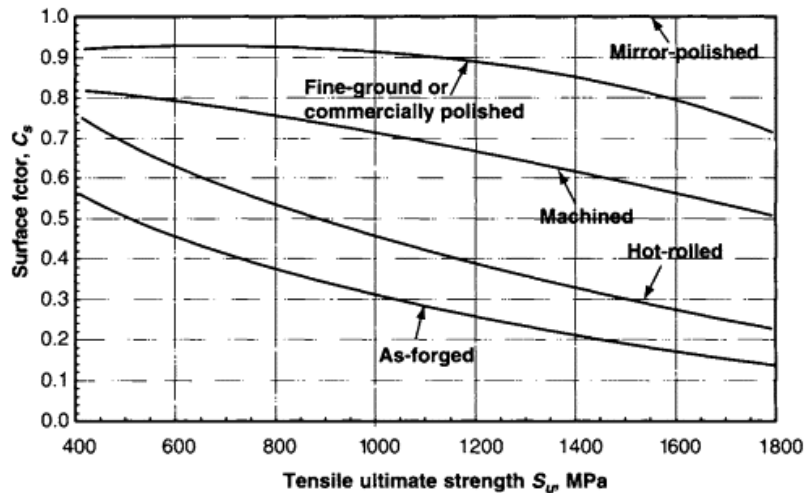
Figure 4.9: Qualitative description of surface finish factor [31]

4.5.1 Effects of surface finishing factors on the surface fatigue

Fatigue is the phenomenon in which a repetitively loaded structure fractures at a load level less than its ultimate static strength. For instance, a Structural steel beam might successfully resist a single static application of a 150 k.N tensile load, but might fail after 10^3 repetitions of a 100 k.N load. The primary factors that contribute to fatigue failures include:

- The number of load cycles experienced.

- Range of stress experienced in each load cycle.

- Mean stress experienced in each load cycle.

- Presence of local surface stress concentrations

A formal fatigue evaluation accounts for each of these factors as it calculates how used up a certain component will become during its anticipated life cycle. Of the four aforementioned primary factors presence of local stress, and concentration is relatively difficult to quantify and many factors that influence the value of these surface roughness and manufacturing process are the main factors and their qualitative description is shown in Figure 4.8 and Figure 4.9 respectively.

Such influencing factors are not directly available in the ANSYS workbench however
there is a factor called fatigue strength factor (K_f). By keeping all other stress concen-
tration factors constant, the fatigue strength factor is set for different manufacturing
methods as shown in Table 4.3.

Table 4.3: Surface roughness and K_f for different manufacturing processes

Manufacturing process	K_f	Surface roughness (μm)
Mirror polished	1	0.05
Fine ground	0.9	12.5
Machined	0.8	25
Hot rolled	0.7	50

The fatigue life of the pair of involute spline meshes are then estimated by changing
those values in the ANSYS workbench as mentioned in Figure 5.7. Then the results
are proposed as shown on the tabular data for fatigue life of the splined shaft for the
different loads and different fatigue strength factors as shown in Table 4.4. For the
sample, the FEA results are shown in Figure 4.10 and Figure 4.11 respectively.
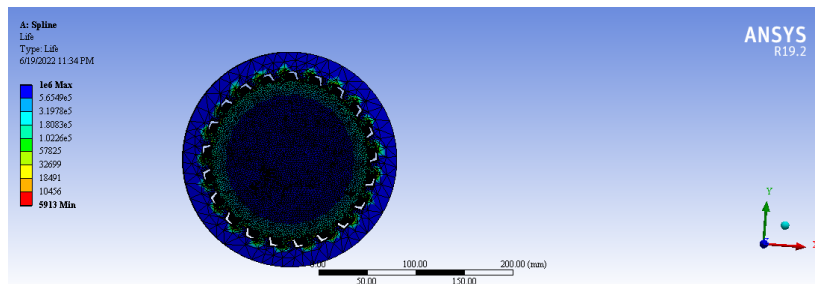
Figure 4.10: Fatigue life at kf=0.7 and at Moment of 150 Nm
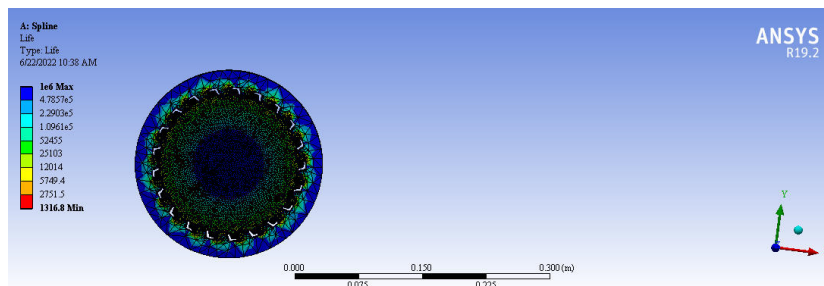
Figure 4.11: Fatigue life at kf=0.7 and at Moment of 1350 Nm

The fatigue life was determined by varying the surface load conditions for the specific

fatigue strength factor to check out the maximum shear stress and Von-misses under fatigue life Von-misses. The Table 4.4 shows the Von-misses and maximum shear stress relations under fatigue tool per life.

As shown in Table 4.4, the maximum shear stress and equivalent (Von-Misses) stress theory are determined for various loading conditions and fatigue strength factors. Meanwhile, most shear stress is more conservative than the Von-Misses theory, see conjointly their variation in Figure 4.10.

Table 4.4: Surface Fatigue life analysis tabular data for all fatigue strength factors

Applied moment and fatigue life under Von misses stress using ANSYS Workbench	
The moment applied [Nm]	Fatigue life using Von misses (ANSYS workbench)
1350	9195.2
1200	16568
1050	29830
900	53667
750	96478
600	173310
450	311080
300	557960
150	1000000

The moment applied and fatigue life with a different K_f				
The moment applied [Nm]	K_f@1.0	K_f@0.9	K_f@0.8	K_f@0.7
1350	6855.4	2700.7	1895.6	1316.8
1200	12780	5210.4	3803.9	2758.4
1050	23878	10052	7633.1	5762.1
900	44582	19349	15288	12036
750	83173	37274	30638	25143
600	155050	71857	61441	52521
450	288830	138630	123290	109710
300	537630	267660	247560	229170
150	1000000	517160	497400	478720

As shown in Figure 4.11, the variations of maximum shear stress and Voin Misses stress versus allowable fatigue life cycles, and the graph was plotted between maximum 10×10^6 and the minimum value of shear stress 0.013168×10^5. The S-N diagram

was plotted by applying the momentum on splined shaft, this shows that clear variation between them. For this graph, the python code is mentioned in the Figure 5.8.
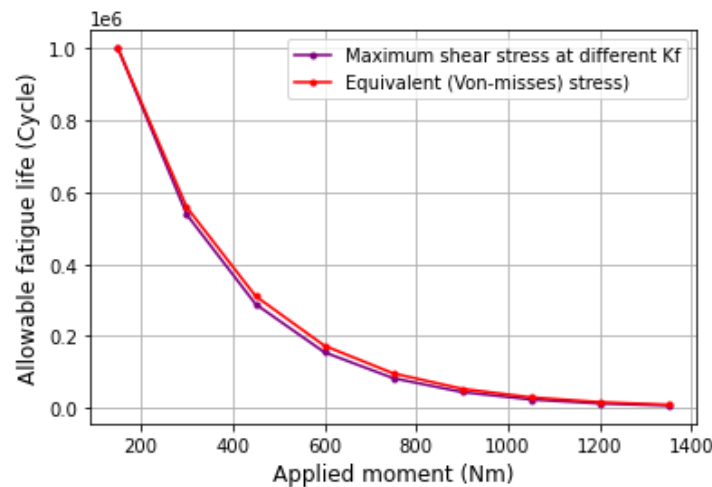
Figure 4.12: Influence of applied mom on fatigue life under Von misses and $\tau_m ax$

Hence, from currently on, the maximum shear stress criteria will be used. It shows the variations of maximum shear stress and Von Misses versus allowable fatigue life cycles. This results gives high concept when the manufacturer finishes the surfaces of the component during the manufacturing process.

4.6 The effects of fatigue strength factor on allowable fatigue life

The surface fatigue or other structural component life is affected by cyclic stresses, residual stresses, material properties, internal defects, grain size deformation, temperature rise, design geometry, surface quality, oxidation, corrosion, etc. But to this study, the surface quality due to surface manufacturing process is taken into account, and all results are considered such activities.

The Fatigue life is the number of cycles of surface loading to failure, the structural internal energy sustains that component load from being a failure. The SN curve (Stress Vs Number of cycles to fail) can be used to predict the fatigue life at cyclic stress that becomes from the surface load for a particular amplitude).

Fatigue strength is the value of stress (S) amplitude for which failure occurs after a particular number of cycles (N). it varies also with the number of cycles required for failure. So, the S-N curve can be used to obtain the fatigue strength required for certain fatigue life, and as the number of cycles increases the fatigue strength factor also increases respectively as shown in Figure 4.13.
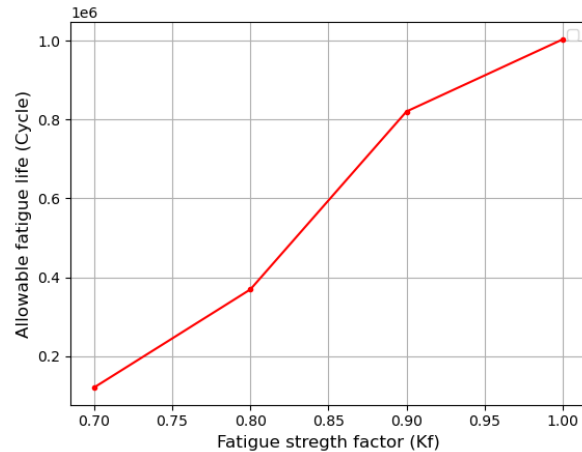
Figure 4.13: Influence of different fatigue strength factors on allowable fatigue life

4.7 The effects of initial surface roughness on surface fatigue life

It is not possible to manufacture a part with a perfectly smooth surface because imperfections and irregularities are bound to occur [1]. They arise in the form of successive hills and valleys. So, the factors affecting the surface roughness are vibration, material quality, type of machining, the rigidity of the machining center, type and material of cutting tool, and cutting conditions like feed, speed, and depth of cut. The surface roughness is to control the surface textures, improve the fatigue resistance, and service life, and reduce initial wear, frictional wear, corrosion, etc. According to Table4.3 information, the effects of initial surface roughness on surface fatigue life are plotted in Figure 4.14 below.
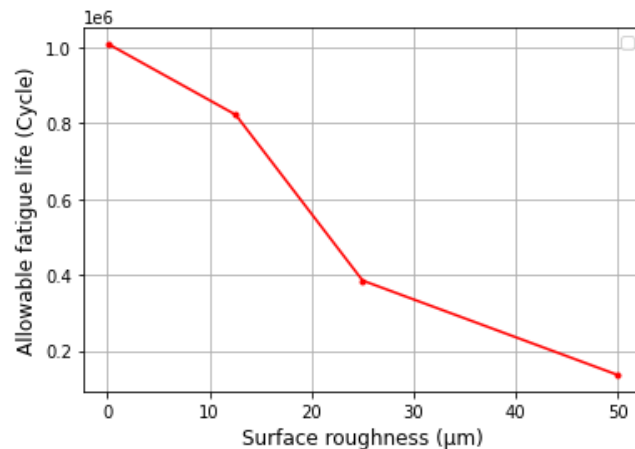
Figure 4.14: Influence of initial surface roughness on surface fatigue life

As shown in the above plotted Figure 4.14, the results showed that surface roughness was a significant factor leading to a short life regime and that fatigue properties decreased when the surface roughness of the component increased.

4.8 Effects of the surface finishing process via the allowable fatigue life cycle

The part is probably characterized by its ability to withstand wear and fatigue, restrict proper lubrication, and increase or decrease friction mating parts. The fatigue strength of a component is known to highly depend on its surface quality, and it is thus necessary to develop a reliable and appropriate mathematical model for fatigue strength assessment that considers the effect of surface roughness.

So, In this study, the surface fatigue life is applied for the moments which varies from 1350 to 150 Nm with different initial surface roughness's has plotted in Figure 4.15. Because of the impact of surface roughness will reduce the fatigue strength of components and might even cause disastrous consequences once the applied load level is below the fatigue limit of the material. The surface finish will have an effect on the power of the part to resist wear and fatigue; to help or destroy effective lubrication; to extend or decrease friction and/or abrasion with mating parts; and to resist corrosion. To all of the four surface finishing process via allowable fatigue life was plotted in the Figure 5.12.
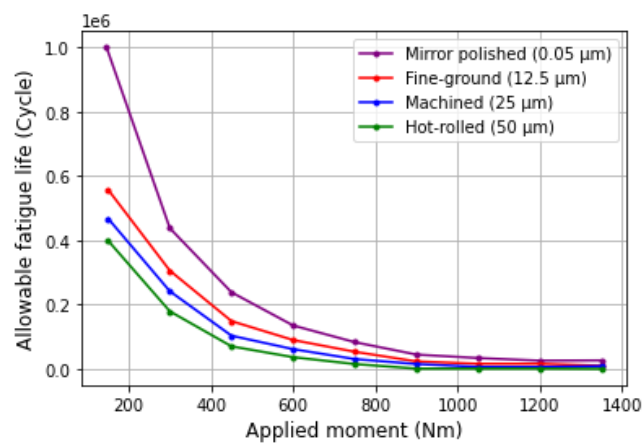
Figure 4.15: Influence of surface finish process with allowable fatigue life cycle

The results showed that when the applied load increases the surface fatigue life will decrease for given initial surface roughness. When the applied moment as the initial surface roughness increases the allowable fatigue life reduces significantly, especially for lower loads. Among the four, mirror polished is has high fatigue life cycle.

5. CONCLUSION, RECOMMENDATION, AND FUTURE WORKS

5.1 Conclusion

This study details surface contact stress of the splined meshes due to varying different surface factor that to be leads to failure. Because the surface quality is known to have a significant impact on a component's fatigue strength, so it is essential to create an accurate and useful mathematical model for determining surface fatigue strength. So, the surface fatigue life for different applied moments which varies from 1350 to 150 Nm with different initial surface roughness's was plotted. Different Fatigue strength factor under fatigue tool and contact tool were applied.

In this study, an agreeable conclusion was reached after comparing the contact stress derived from Hertz-man's stress theory with the contact stress derived from the finite element analysis, and those are validated with experimental investigations called photo-elasticity. The contact stress is the same in both FEM and Hertzian, with a minimal variance of 5.9%.

The variation of contact stress with various influence of factors was also compared and it was used to estimate the surface fatigue life and examine the impact of altering the coefficient of friction on contact stress. From such results, when the coefficient of friction increased on pair surface maximum contact stress is also increased, it give high consideration surface finishing process.

Finally, the impact of various surface finish factors was examined. When the applied load increases the surface fatigue life will decrease for given initial surface roughness. Different fatigue strength factor is also analyzed for the different applied moment (surface loading conditions), the results showed that when the fatigue strength factor is increased the life cycle of the moment applied is inversely decreased.

5.2 Recommendation

- Based on the results from the surface fatigue stress analysis, the hardness of the splined meshes of involute profiles should be improved to resist surface pitting failure.

- The degree of frictional coefficient effects on contact stress depends on the coefficient of friction of contact surface roughness and input torque. This shows that good surface finishing leads to less coefficient of friction and high life existence.

- In actual surface manufacturing processes, frictional effect has a substantial impact on production performance.

  – So, designers should give more attention to minimizing or utilizing surface frictional effects by considering all the results of surface finishing processes with their roughnesses.

- The Finite element analysis takes less time and is less expensive than the experimental method, and the parametric study for such contact stress can be used where the experimental setup is not available.

5.3 Future Works

This study has been conducted with a miniaturized involute splined shaft and hub connection. The following areas were not considered on this study, such as;

- When the two components move together, thereafter temperature will be created, this effect of contact temperature leads to surface leaking and small pitting.

- The hardness of the flank surface of the component may resist failure due to the acting load. To do so, varying composite materials optimization for such activities should consider.

- To carry away heat generated inside the bearing due to friction and other causes, the consideration of effects of lubrication is very important.

Bibliography

[1] Sandor Bodzas, Manufacturing of the surfaces of spline fitting connection, *The International Journal of Advanced Manufacturing Technology*, Vol 111, No. 01, pp. 909-920, Jul 2020. ISSN: 2502-4752.

[2] Govindarajan Narayanan, Effect of sliding friction on spline surface failure under misaligned condition in aero engines, *International Journal of Structural Integrity*, vol 07, No. 05, pp. 617–629, Sept 2016, DOI: http://dx.doi.org/10.1108/IJSI-07-2015-0024.

[3] Francesca Cura, Andrea Mura, and Federica Adamo, Fatigue damage in spline couplings: Numerical simulations and experimental validation,*Procedia Structural Integrity*, vol 05, pp. 1326–1333, Nov 2017, ISSN: 2452-3216, DOI: 10.1016/j.prostr.2017.07.141.

[4] Tumpala Uma Santhosh, R.Arti Babu, A.Vinutha, and P.N.Sharma, Analysis of Spline Profile and Its Manufacturing, *International Journal of Latest Engineering Research and Applications (IJLERA)*, vol. 01, No. 09, pp. 17–43, Dec 2016, ISSN: 2455-7137.

[5] Dhananjay Ghanshyam Pardhi and S D Khamankar, Stress analysis of spline shaft using Finite Element Method and its experimental verification by photoelasticity, *International Journal of Mechanical Engineering and Robotics Research(IJMERR)* vol 3, No. 4, pp. 451–458, Oct 2014, DOI: 10.18178/ijmerr.

[6] DA. Wei Zhang, Die structure and its trial manufacture for thread and spline synchronous rolling process, *International Journal of Advanced Manufacturing Technology*, DOI: pp: 319–325, Jan 2018, https://DOI.org/10.1007/s00170-2018-1619-4

[7] Rabish Kumar and Nitish Kumar Singh, A Comprehensive Report on the thermal, static and dynamic behavior of spline shaft, *International Journal for Scientific Research and Development*, vol 7, No. 01, pp. 3–8, Apr 2019, DOI:10.13140/RG.2.2.35055.07849.

[8] Swapnil B.Patil and S.R.Patil, Experimental and numerical analysis of a load distribution along the length of contact in involute spline shaft, *International Journal*

of Advanced Technology and Engineering Exploration, vol 6, No. 51, pp. 30–44, Feb 2019, DOI: 10.19101/ijatee.2019.650006.

[9] José Francisco and Ramos Teixeira, American standard ANSI B921-1996 involute splines and inspection pitch, *Society of automotive Engineers*, pp 15096-0001 Oct 2020.

[10] J. Hong, D. Talbot, and A. Kahraman, A semi-analytical load distribution model for side-fit involute splines, *Mechanism and machine theory*, vol 76, pp. 39–55, Feb 2014, DOI: 10.1016/j.mechmachtheory.2014.02.002, 0094-114X.

[11] J. Hong, D. Talbot, and A. Kahraman, Load distribution analysis of clearance-fit spline joints using finite elements, *Mechanism of machinery theory*, vol 74, pp. 42–57, Apr 2014, DOI: 10.1016/j.mechmachtheory.2013.11.007.

[12] H.Wiang. Li and X. Bin Wang, New measurement method for spline shaft rolling performance evaluation using laser displacement sensor, *Chinese Journal of Mechanical Engineering (CJME)*, vol 31, No. 4, Oct 2018, DOI: 10.1186/s10033-2018-0265-y.

[13] A. Stenstrand, Spline optimization tool using Finite Element Analysis, *chalmers university of technology*, vol 05, pp: 96-412, Jun 2018, DOI: http://publications.lib.chalmers.se/records/fulltext/256372/256372.

[14] L.H.Zhao, Q.K.Xing, J.Y.Wang, S.L.Li, and S.L.Zheng, Failure and root cause analysis of vehicle drive shaft, *Engineering Failure Analysis*, vol 99, No.3, pp. 225–234, Feb 2019, DOI: 10.1016/j.engfailanal.2019.02.025.

[15] B. Engel, Sara Salman Hassan, and Al-Maeeni Failure Analysis and Fatigue Life Estimation of a Shaft of a Rotary Draw Bending Machine, *International Journal of Innovation Science and Research* , vol 11, No. 11, pp. 1785–1790, Feb 2017, ISSN: 2319-9369

[16] Tae-Wan Ku, A study on two-stage cold forging for a drive shaft with internal spline and spur gear geometries, *Metals*, *the Portuguese Society of Materials (SPM)*, vol. 8, No. 11, Nov 2018, DOI: 10.3390/met8110953.

[17] Minchao Cui, Shengdun Zhao, Chao chen, Dawei Zhang, and Yongyi Li, Finite element modeling and analysis for the integration-rolling-extrusion process of spline shaft, *Advances in Mechanical Engineering (AIME)*, vol. 09, No. 2, pp. 1–11, Feb 2017, DOI: 10.1177/1687814016688585.

[18] Francesca Cura and Andrea Mura, Evaluation of the fretting wear damage on crowned splined couplings, *Elseveir/Engineering failure analysis*, vol 131, Sep 2017, pp. 1393-1400, ISSN: 1350-6307, DOI: https://10.1016/j.prostr.2017.07.203

[19] O. Lyashuk and Yuriy Pyndus, Fracture cause analysis of the extruder's shaft and geometry optimization of the spline, *Journal of Mechanical Engineering and Sciences*, vol. 13, No. 1, pp. 4449–4460, Mar 2019, DOI: 10.15282/jmes.13.1.2019.08.0378.

[20] Felix Muller, S. Schumann, and B. Schlecht, Innovative tooth contact analysis with non-uniform rational b-spline surfaces, *Forsch Ingenieurwes/Engineering*, vol. 03, No. 2, Sep 2021, DOI: 10.1007/s10010-021-00521-7.

[21] Yuan Chen, Yabing Liao, Maohua Xiao,Wei Zhang, Guanghu Jin, Fretting wear analysis of spline couplings in agricultural tractor with axis deviation, *Journal of Vibro engineering (JVE)*, Vol. 22, No. 05, Feb 2020, pp. 1165-1173, DOI: https://doi.org/10.21595/jve.2020.21304.

[22] Kashid Vishal R.Mane and Ashwini M, Finite element analysis and optimization of tractor trolley axle, *International Journal of Engineering Research and Applications (IJERA)* vol 07, Apr 2016, pp. 48-60.

[23] Yong Hu, David Talbot, and Ahmet Kahraman, A Gear load distribution model for a Planetary gear set with a flexible ring gear having external splines, *American Society of Mechanical Engineers*, vol 11, Jan 2019, pp. 18-1604, DOI: https://doi.org/10.1115/1.4041583

[24] V. Singh, P. Atul, and K. Soni, Experimental and Computational Analysis of Lathe Spline Shaft - A Comprehensive Report, *International Journal for Scientific Research and Development*, vol 7, No. 07, pp. 79–84, Feb 2019, ISSN: 2321-0613

[25] Ning-yu Ben, Qi Zhang, and Da-wei Zhang, Improvement of axial forging process for spline shaft by die design, *International Journal of Advanced Manufacturing Technology*, vol 99, No. 9–12, pp. 2727–2741, Sept 2018, DOI: 10.1007/s00170-018-2594-5.

[26] Noureddine Barka, Sasan Sattarpanah Karganroudi, Rachid Fakir, Patrick Thibeault, and Vincent Blériot Feujofack Kemda, Effects of laser hardening process parameters on hardness profile of 4340 steel spline an exper-

imental approach, *MDPI/Coatings*, vol 10, No 4, pp. 10-342, Apr 2020.
https://doi.org/10.3390/coatings10040342

[27] L. Gang and S. Yong, Fatigue Life Calculation of Shaft System Based on Bend-Torsion Coupling, *IOP Conference Series/ Materials Science and Engineering*, vol 569, No. 2, Jul 2019, DOI: 10.1088/1757-899X/569/2/022008.

[28] Kalathur Kumar, Dr.S.Arul, Dr.G.Sriram, Dr.V.N.Mani, and V.Prathap Kumar, Investigation of pitting formation on gear tooth and evaluating life time of gears using SEM, *Engineering/Materials Science* vol 03, No. 64, Dec 2016, pp. 2393-8374, DOI: https://doi.org/10.1515/mt-2158.

[29] Suresh P.M, Mruthunjaya M., Root cause of analysis of forged spline yoke shaft using Finite Element Method, *Materials Today: Proceedings*, Vol 05, No. 10, Aug 2018, pp. 23491–23498, DOI: https://doi.org/10.1016/j.matpr.2018.10.136

[30] L.j Shen, A. Lohrengel, and G. Schafer, Plain fretting fatigue competition and prediction in spline shaft-hub connection, *Materials and Design*, Vol 52, pp. 68-81, Feb 2014, ISSN: 0142-1123, DOI: https://doi.org/10.1016/j.ijfatigue.2014.11.012.

[31] G. Adams, and Robert W. Bruce, Contact mechanics/Handbook of Lubrication and Tribology, theory and design, *Taylor and Francis group* Vol. 02 , Second Edition. pp. 4–20, May 2012, ISBN: 97814-20069082, DOI: 10.1201/b12265.

[32] Tumpala uma santosh, A.Vinutha, and P.N.Sharma, Analysis of spline profile and its manufacturing, *International Journal of Latest Engineering Research and Applications (IJLERA)*, Vol 01, Jul 2016, pp. PP 17-43, ISSN: 2455-7137.

[33] Budynas Nisbett, Shigleys Mechanical Engineering Design, *McGraw Hill Companies/United states of America*, Vol 01, Eighth Edition, Jul 2008, pp. 550-711, http://www.primisonline.com

[34] P Maurya, N Mulani, C Michael1 and D Jebaseelan, Failure analysis of drive axle shaft failed under Torsional stress, *Materials Science and Engineering*, Vol. 05, Oct 2021, DOI: https://doi.org/10.1088/1757-899x/1128/1/012011.

[35] Benatar, M., Talbot, D. and Kahraman A., An experimental investigation of the load distribution of splined joint under gear load conditions, *Journal of Advanced Mechanical Design*, *Systems*, *and Manufacturing*, Vol 11, No. 06, Sep 2017. pp. 17-00203, DOI: https://doi.org/10.1299/jamdsm.2017jamdsm0084

[36] CNHTC, CNPC, and CHC, HOWO dump truck Product description and specification, *SinotrukHowo.cn*, spec- 06, Aug 2015. website: https://sinotrukhowo.cn/portfolio-item/howo-dump-truck/

[37] ANSYS Inc., and Southpointe, ANSYS Contact Technology Guide, *ANSYS, Inc.*, Vol 09, November 2014, PP. 45-84, ISO: 9001 website: https://www.cae.tntech.edu/ chriswilson/FEA/ANSYS/gctec90

[38] Clement Dupertuis and Ligier JL, Contact pressure in misaligned spline couplings, *Mechanics and Industry*, vol 21, Jan 2020, DOI: https://doi.org/10.1051/meca/2020049

[39] Max Weibring, Leonard Gondecki, Peter Tenberge, Simulation of fatigue failure on tooth flanks in consideration of pitting initiation and growth, *Elseveir/Tribology International*, Vol. 131, Oct 2018, pp. 299-307 https://doi.org/10.1016/j.triboint.2018.10.029

[40] M.F.AL-Mayali, S. Hutt, K.J.A. Clarke, and H.P.Evans Sharif, Experimental and numerical study of micro-pitting initiation in real rough surfaces in a micro elasto hydrodynamic lubrication regime, *Springer/Tribology Letters*, vol. 66, No. 150, Nov 2018, https://doi.org/10.1007/s11249-018-1110-2

[41] Vincenzo Cuffaro, Francesca Cura, and Andrea Mura, Surface characterization of spline coupling teeth subjected to fretting wear, *International Colloquium on Mechanical Fatigue of Metals/Procedia Engineering*, vol. 174 No. 13, Oct 2014, pp. 135–142, https://creativecommons.org/licenses/by-nc-nd/3.0/

[42] Xiangzhen Xue, Sanmin Wang, and Bo Li, Modification methodology of fretting wear in involute spline, *Elseveir/wear/School of Mechanical Engineering, Northwestern Poly-technical University*, vol. 368-369, No. 123, Aug 2016, pp. 435–444, https://doi.org/10.1016/j.wear.2016.10.015

[43] Yi Guoa, Scott Lambert, Robb Wallen, and Robert Errichello, Jonathan Keller, Theoretical and experimental study on gear-coupling contact and loads considering misalignment, torque, and friction influences, *Elseveir/Mechanism and machine theory*, vol. 98, No. 98, Apr. 2016, pp. 242–262, DOI: https://doi.org/10.1016/j.mechmachtheory.2015.11.015

Appendix-A: Pressure angle formulae as ANSI B92.1 manual

The following Figure, details interconnection for the pressure angle of 30, 37.5, and 45 degrees. They are more common angles for the application of such components. Which is derived from ANSI B92.1 manual of involute spline shaft and hub and shown in Figure 5.1

Term	Symbol	Formula			
		30° Flat Root Side Fit 2.5/5 thru 32/64 Spline Pitch	**30°** Fillet Root Side Fit 2.5/5 thru 48/96 Spline Pitch	**37.5°** Fillet Root Side Fit 2.5/5 thru 48/96 Spline Pitch	**45°** Fillet Root Side Fit 10/20 thru 128/256 Spline Pitch
Stub Pitch	P_s	$2P$	$2P$	$2P$	$2P$
Pitch Diameter	D	$\dfrac{N}{P}$	$\dfrac{N}{P}$	$\dfrac{N}{P}$	$\dfrac{N}{P}$
Base Diameter	D_b	$D \cdot \cos\phi$	$D \cdot \cos\phi$	$D \cdot \cos\phi$	$D \cdot \cos\phi$
Circular Pitch	p	$\dfrac{\pi}{P}$	$\dfrac{\pi}{P}$	$\dfrac{\pi}{P}$	$\dfrac{\pi}{P}$
Minimum Effective Space Width	s_v	$\dfrac{\pi}{2P}$	$\dfrac{\pi}{2P}$	$\dfrac{0.5\pi + 0.1}{P}$	$\dfrac{0.5\pi + 0.2}{P}$
Major Diameter, Internal	D_{ri}	$\dfrac{N+1.35}{P}$	$\dfrac{N+1.8}{P}$	$\dfrac{N+1.6}{P}$	$\dfrac{N+1.4}{P}$
Major Diameter, External	D_o	$\dfrac{N+1}{P}$	$\dfrac{N+1}{P}$	$\dfrac{N+1}{P}$	$\dfrac{N+1}{P}$
Minor Diameter, Internal	D_i	$\dfrac{N-1}{P}$	$\dfrac{N-1}{P}$	$\dfrac{N-0.8}{P}$	$\dfrac{N-0.6}{P}$
Minor Diameter, External — 2.5/5 thru 12/24 spline pitch	D_{re}			$\dfrac{N-1.8}{P}$	
Minor Diameter, External — 16/32 spline pitch, and finer	D_{re}	$\dfrac{N-1.35}{P}$	$\dfrac{N-2}{P}$	$\dfrac{N-1.3}{P}$	
Minor Diameter, External — 10/20 spline pitch, and finer	D_{re}				$\dfrac{N-1}{P}$
Form Diameter, Internal	D_{fi}	$\dfrac{N+1}{P} + 2c_F$	$\dfrac{N+1}{P} + 2c_F$	$\dfrac{N+1}{P} + 2c_F$	$\dfrac{N+1}{P} + 2c_F$
Form Diameter, External	D_{fe}	$\dfrac{N-1}{P} - 2c_F$	$\dfrac{N-1}{P} - 2c_F$	$\dfrac{N-0.8}{P} - 2c_F$	$\dfrac{N-0.6}{P} - 2c_F$
Form Clearance (Radial)	c_F	0.001D, with max of 0.010, min of 0.002			

Figure 5.1: Formulae for involute spline geometry based on ANSI 92.1

Appendix-B1: Surface Finishing for various manufacturing processes

Surface finishes vary hugely by the producing method accustomed to them. A flame-cut plate edge contains a radically different surface finish than a ground surface, for instance. Selecting a method that's capable of achieving the required surface finish is the start of working out the way to manufacture a part that needs a selected finish. Sometimes, more than one method should be employed to attain the required result cost-effectively. Here's a chart showing the relative surface finish roughness of various manufacturing processes as shown in Figure 5.2
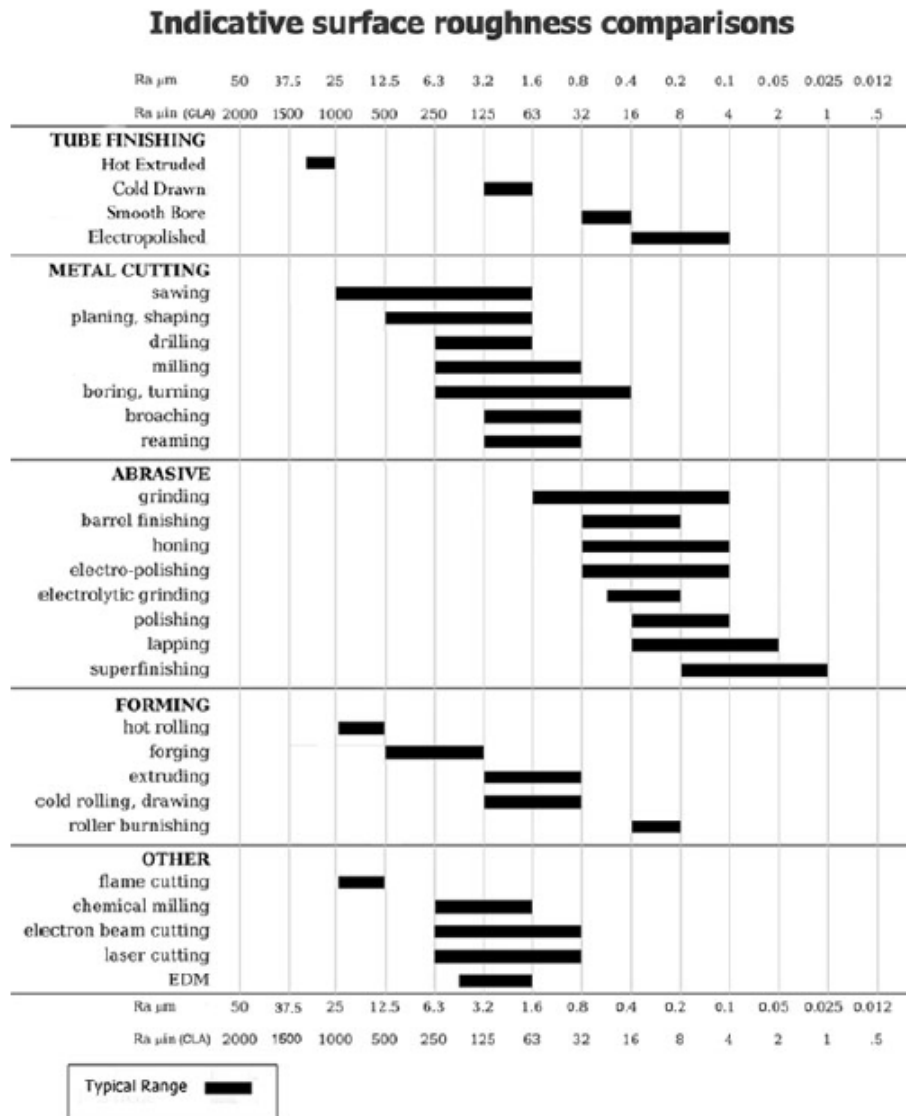

Figure 5.2: Indicative surface roughness parameters

Appendix-B2: Mesh-type element descriptions for the numerical Application

- **CONTA174 Element geometry description**

This part description is employed to represent contact and sliding between 3-D target surfaces and a deformable surface outlined by this part. The part applies to 3-D structural and coupled-field contact analyses. It may be used for each pair-based contact and genera contact. The part is found on the surfaces of 3-D solid or shell components with mid-side nodes (SOLID87, SOLID90, SOLID98, SOLID122, SOLID123, SOLID186, SOLID187, SOLID226, SOLID227, SOLID232, SHELL132, SHELL281, and MATRIX50).

The part has identical geometric characteristics because the solid or shell part face with that it's connected as shown in Figure 5.3. Contact happens once the part surface penetrates one among the target phase components (TARGET170) on such target surface. Coulomb friction, shear stress friction, user-outlined friction with the USER-FRIC software system, and user-defined contact interaction with the user interface software system area unit are allowed. The part additionally permits the separation of secured contact to simulate interface delamination. See CONTA174 in Appendix D underneath Section II.
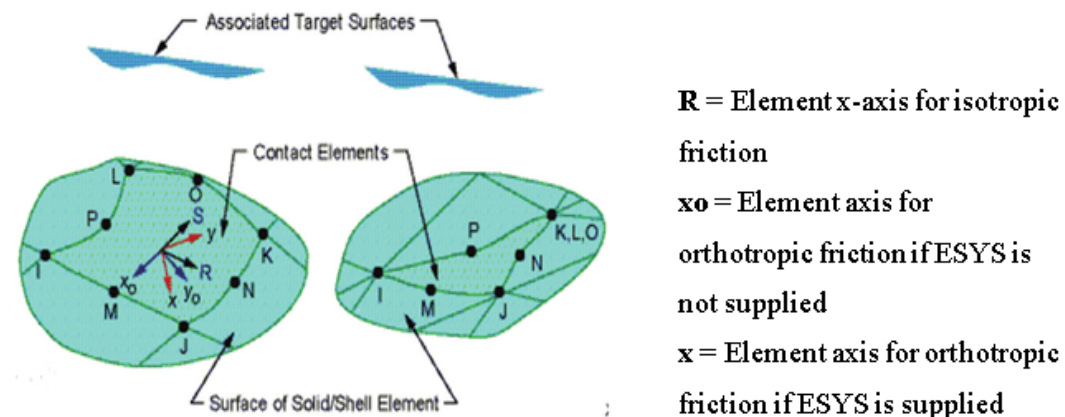

Figure 5.3: CONTA174 Element geometry

 • **TARGE170 Element Description**

TARGE-170 is employed to represent numerous three-D target surfaces for the associated contact parts (CONTA173, CONTA174, CONTA175, CONTA176, and CONTA177). The contact parts themselves overlay the solid, shell, or line elements describing the boundary of a deformable body and are potentially in-tuned with the target surface, as defined by TARGE-170. This target surface is discretized by a collection of target phase parts (TARGE-170) and is paired with its associated contact surface via a shared real constant set. you'll impose any travel or motility displacement, temperature, voltage, and magnetic potential on the target phase component. you'll additionally impose forces and moments on track parts. See TARGE170 in Appendix II for a lot of details concerning this component. To represent 2-D target surfaces, use TARGE169, a 2-D target phase component.

For rigid target surfaces, these parts will simply model complicated target shapes. For versatile targets, these parts can overlay the solid, shell, or line parts describing the boundary of the deformable target body.
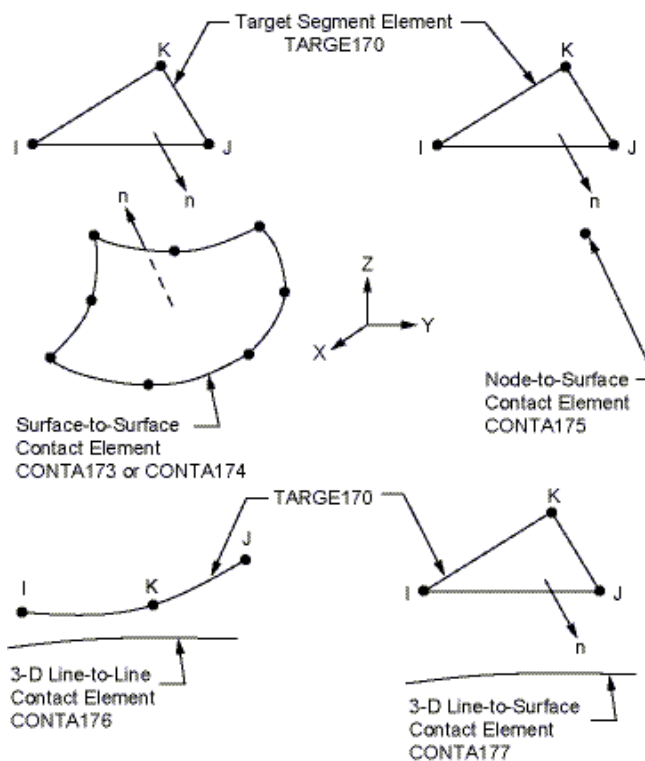

Figure 5.4: CONTA170 Element geometry

Appendix-C: Pressure distribution along the contact surfaces

The following python code used for analyzing the relationship between the contact pressure distribution and area to the surface to surface contact for the Equation, as mentioned on the Equation 3.3 and 3.6.

```python
 1
 2              #  Pressure Distribution along the area of the contact surfaces
 3
 4      import numpy as np
 5      import matplotlib.pyplot as plt
 6
 7      # p - contact pressure
 8      # a - surface contact area wrt to contact pressure
 9      # E - Equivalent Young's modulus of elasticity, take as (E*)
10      # R - Radius of realtive curvature, take as (R* or R)
11
12      # Sample user input parameters are given below, which is for max torque only
13
14      E = 8.835e12   #..... (From the equation of 3.6, chapter three)
15      p = 28.763
16      R = 16.667      #..... (From the equation of 3.6, chapter three)
17      pi = 3.14      # radian value
18
19      a = (4*((p*R)/(4*np.pi*E))**1/2)
20      print(a,9)
21      x = np.linspace(-a,a,9)
22      print(x)
23
24      p=(((p*E)/(np.pi*R))-(x**2*E**2/(4*R**2)))**0.5 #Local pressure distribution
25      print(p)
26      plt.plot(x,p, label = 'determination of maximum contact pressure due to contact area',
27              marker="" , color="green")
28      plt.xlabel ("Contact area (a) mm^2" , fontsize=14 , color='black')
29      plt.ylabel ("Contact pressure (p) N/mm^2" , fontsize=12 , color='black')
30      plt.plot(x,p)
31      plt.grid()
```

Figure 5.5: The distribution of the surface pressure on the spline surface

Appendix-D: Arrays for the Hertz contact stress and moment of applied

The array of the moment of application which is derived from the engine to the rear wheel and hertz surface contact stress for the flank face of the component of the array is developed on the Jupyter notebook. It s used to also plot the graph with the relation of that moment of applied torques and its contact stress.

```python
import numpy as np
from sympy import *
import matplotlib.pyplot as plt


        # Nomenclature for each terms

#HCS - Hertizean stress analysis
#R1 and R2 - are pich radius of pinion and gear respectively
#B - is the face width of the spline
#phi - is the pressure angle, its 30 degrees for the involute spline
#v1 and v2 - is the poisson ratio of pinion and gear respectively
#E1 and E2 - are the modules of elasticity of pinion and gear
#Mom - moment applied in N.m
# assume the radii of hub and splined shaft are equal
# assume the material of the hub and shaft are same
#F - is the force applied
            # Sample user input values are given below
Mom = 1350 Nm = 1350*(10)**1/3) Nmm
R1 = (Dp/2) = R2 = 30
pi = 3.1416
B = 0.02618 = (pi/(2*P))|
V1 = 0.3 = V2 = 0.3
E1 = 206e9 = E2 = 206e9
phi = 30 degrees = (30*(pi/180)) = 0.5236 radian

Mom = np.linspace(150,1350,9, retstep=True)
print(Mom)
F = Mom/R1 = Mom/R2;
HCS = ((F*(1+(R1/R2)))/R1*B*pi[((1-(V1**2)/E1)+((1-(V2**2))/E2)]*sin(phi))
print(HCS)
```

```
(array([ 150.,  300.,  450.,  600.,  750.,  900., 1050., 1200., 1350.]), 150.0)
```

Figure 5.6: Array Jupyter notebook code for Hertz's contact stress and applied moment

Appendix-E: Maximum shear stress on different fatigue strength factors under fully reversed loading conditions

Figure 5.7: Maximum shear stress for fully reverse loading conditions on different fatigue strength factors

Appendix-F: Python code for equivalent Voin Misses and shear stress

```python
#Maximum shear stress and Equivalent (Von-misses) stress relations

import numpy as np
import matplotlib.pyplot as plt
xi=(150,300,450,600,750,900,1050,1200,1350)
yi=(10*10**5,5.376*10**5,2.8883*10**5,1.5505*10**5,0.83173*10**5,0.4458*10**5,0.2388*
xj=(150,300,450,600,750,900,1050,1200,1350)
yj=(10*10**5,5.57960*10**5,3.11080*10**5,1.73310*10**5,0.96478*10**5,0.53667*10**5,0.
plt.plot(xi,yi, label="Maximum shear stress at different Kf", marker="." , color="pur
plt.plot(xj,yj, label="Equivalent (Von-misses) stress)", marker="." , color="red")
plt.xlabel ("Applied moment (Nm)" , fontsize=12)
plt.ylabel ("Allowable fatigue life (Cycle)" , fontsize=12)
plt.legend( )
#plt.figure(figsize=(9,9))
#plt.show()
plt.grid()
```

Figure 5.8: Maximum shear stress and equivalent Voin Misses stress relations code

```python
#    Allowable fatigue life cycle vs Fatigue stregth factor

import numpy as np
import matplotlib.pyplot as plt

x=(0.7,0.8,0.9,1)
y=(0.1209*10**6,0.3692*10**6,0.8203*10**6,1.003*10**6)

plt.plot(x,y, label="", marker="." , color="red")
plt.xlabel("Fatigue stregth factor (Kf)" , fontsize=12 , color="black")
plt.ylabel("Allowable fatigue life (Cycle)" , fontsize=12 ,  color="black")

plt. legend()
plt.grid( )
#plt. show()
```

Figure 5.9: Allowable fatigue life via fatigue strength factor code

Appendix-G: Python code for contact stress validation

```
#Graphical Validation for Analytical method, Numerical(ANSYS Workbench), and Experimental
          #LIBRARY
import numpy as np
import matplotlib.pyplot as plt

       #1. Hertz Results

x1=(150,300,450,600,750,900,1050,1200,1350)
y1=(0.527*10**6,1.021*10**6,1.459*10**6,1.915*10**6,2.141*10**6,2.350*10**6,2.534*10**6,2.

       #2. Numerical Results

x2=(150,300,450,600,750,900,1050,1200,1350)
y2=(0.5408*10**6,1.0816*10**6,1.6224*10**6,2.1632*10**6,2.704*10**6,3.248*10**6,3.785*10**

       #3. Experimental Investigations

x3=(150,300,450,600,750,900,1050,1200,1350)
y3=(0.515*10**6,0.972*10**6,1.289*10**6,1.596*10**6,1.779*10**6,2.046*10**6,2.278*10**6,2.

       #PLOTTING GRAPH

plt.plot(x1,y1, label="Contact stress (Hertzian formulae)", marker="." , color="blue")
plt.plot(x2,y2, label="Contact stress (Numerical analysis)", marker="." , color="red")
plt.plot(x3,y3, label="Contact stress (Experimental investigations)", marker="." , color="

plt.xlabel ("Applied moment (Nm)" , fontsize=12)
plt.ylabel ("Contact stresses (Pa)" , fontsize=12)
plt.legend( )
plt.grid()
#plt.figure(figsize=(9,9))
#plt.show()
```

Figure 5.10: Comparison analysis for analytical, numerical, and exp'tal results code

Appendix-H: The percentage error plots for for three contact stress validation

```
1
2    #Spyder code for the percentage deviation analysis of ana, num, and exp'tal works
3
4    import numpy as np
5    import matplotlib.pyplot as plt
6
7    L=(1350,1200,1050,900,750,600,450,300,150)
8    P= (5.91,6.36,6.79,7.33,7.92,8.46,8.99,9.44,9.74)
9
10    #Where, L-load, and P- Percentage varaitions
11
12   plt.plot(L,P, label="", marker="." , color="red")
13   plt.xlabel("Applied Moment (Nm)" , fontsize=12 , color="black")
14   plt.ylabel("Percentage error (%)" , fontsize=12 ,  color="black")
15   plt. legend()
16   plt.grid( )
17   plt. show()
```

Figure 5.11: percentage error among three contact stress

Appendix-I: Python code for effects of surface finshing process and surface roughnesses values dueto surface loading conditions

```python
1    # Plotting for Surface finishing process with surface finishing factor roughness values
2
3    import numpy as np
4    import matplotlib.pyplot as plt
5
6    import numpy as np
7    import matplotlib.pyplot as plt
8
9    x1= (150,300,450,600,750,900,1050,1200,1350)
10   y1= (1*10**6,0.43763*10**6,0.2383*10**6,0.13505*10**6,0.083173*10**6,0.044582*10**6,0.033878*
11
12
13
14   x2= (150,300,450,600,750,900,1050,1200,1350)
15   y2= (0.55716*10**6,0.30566*10**6,0.14863*10**6,0.089857*10**6,0.053274*10**6,0.02335*10**6,0.
16
17
18   x3= (150,300,450,600,750,900,1050,1200,1350)
19   y3=(0.4674*10**6,0.241560*10**6,0.103290*10**6,0.061441*10**6,0.030638*10**6,0.015288*10**6,0
20
21
22   x4=(150,300,450,600,750,900,1050,1200,1350)
23   y4=(0.39872*10**6,0.179170*10**6,0.070210*10**6,0.036521*10**6,0.015143*10**6,0.001036*10**6,
24
25
26   plt.plot(x1,y1, label="Mirror polished (0.05 µm)", marker="." , color="purple")
27   plt.plot(x2,y2, label="Fine-ground (12.5 µm)", marker="." , color="red")
28   plt.plot(x3,y3, label="Machined (25 µm)", marker="." , color="blue")
29   plt.plot(x4,y4, label="Hot-rolled (50 µm)", marker="." , color="green")
30
31   plt.xlabel ("Applied moment (Nm)" , fontsize=12)
32   plt.ylabel ("Allowable fatigue life (Cycle)" , fontsize=12)
33   plt.legend( )
34   plt.grid( )
35   #plt.figure(figsize=(9,9))
```

Figure 5.12: Surface finishing process with its roughnesses

Appendix-J: Python code for Coefficient of frictions for max SLCs

```python
1
2    #Different coefficient of friction results at maximum surface loading condition at 1350 Nm
3
4
5    import numpy as np
6    import matplotlib.pyplot as plt
7
8    x= (0.01,0.05,0.10,0.15,0.20,0.25)
9    y= (4.9271*10**6,4.9089*10**6,4.8887*10**6,4.8670*10**6,4.848*10**6,4.8298*10**6)
10
11   plt.plot(x,y, label="Coefficient of friction @1350 Nm", marker="." , color="red")
12   #plt.title("stress-strain diagram for coefficient of factors")
13   plt.xlabel("Different coefficient of friction")
14   plt.ylabel("Maximum contact stress (Pa)")
15   plt. legend ()
16   plt.grid()
17
```

Figure 5.13: Coefficient of friction under maximum loading loading condition